

This discussion paper is/has been under review for the journal Atmospheric Chemistry and Physics (ACP). Please refer to the corresponding final paper in ACP if available.

Intercomparison and evaluation of aerosol microphysical properties among AeroCom global models of a range of complexity

G. W. Mann^{1,2}, K. S. Carslaw², C. L. Reddington², K. J. Pringle^{2,5}, M. Schulz³,
A. Asmi⁴, D. V. Spracklen², D. A. Ridley^{2,6}, M. T. Woodhouse^{2,25}, L. A. Lee²,
K. Zhang^{7,8}, S. J. Ghan⁸, R. C. Easter⁸, X. Liu^{8,37}, P. Stier⁹, Y. H. Lee^{10,13},
P. J. Adams¹⁰, H. Tost^{5,32}, J. Lelieveld^{5,12}, S. E. Bauer^{11,13}, K. Tsigaridis^{11,13},
T. P. C. van Noije¹⁴, A. Strunk¹⁴, E. Vignati¹⁵, N. Bellouin¹⁶, M. Dalvi¹⁷,
C. E. Johnson¹⁷, T. Bergman¹⁸, H. Kokkola¹⁸, K. von Salzen¹⁹, F. Yu²⁰, G. Luo²⁰,
A. Petzold^{21,33}, J. Heintzenberg²², A. Clarke²³, J. A. Ogren²⁴, J. Gras²⁵,
U. Baltensperger²⁶, U. Kaminski²⁷, S. G. Jennings²⁸, C. D. O'Dowd²⁸,
R. M. Harrison^{29,34}, D. C. S. Beddows²⁹, M. Kulmala³⁰, Y. Viisanen⁴,
V. Ulevicius³¹, N. Mihalopoulos³⁵, V. Zdimal³⁶, M. Fiebig³⁸, H.-C. Hansson³⁹,
E. Swietlicki⁴⁰, and J. S. Henzig⁴¹

¹National Centre for Atmospheric Science, University of Leeds, Leeds, UK

Title Page	Introduction
Abstract	References
Conclusions	Tables
Tables	Figures
	
	
Back	Close
Full Screen / Esc	
Printer-friendly Version	
Interactive Discussion	

**AEROCOM
microphysics
intercomparison**

G. W. Mann et al.

[Title Page](#)[Abstract](#)[Introduction](#)[Conclusions](#)[References](#)[Tables](#)[Figures](#)[|◀](#)[▶|](#)[◀](#)[▶|](#)[Back](#)[Close](#)[Full Screen / Esc](#)[Printer-friendly Version](#)[Interactive Discussion](#)

**AEROCOM
microphysics
intercomparison**

G. W. Mann et al.

[Title Page](#)[Abstract](#)[Introduction](#)[Conclusions](#)[References](#)[Tables](#)[Figures](#)[|◀](#)[▶|](#)[◀](#)[▶](#)[Back](#)[Close](#)[Full Screen / Esc](#)[Printer-friendly Version](#)[Interactive Discussion](#)

Abstract

Many of the next generation of global climate models will include aerosol schemes which explicitly simulate the microphysical processes that determine the particle size distribution. These models enable aerosol optical properties and cloud condensation nuclei (CCN) concentrations to be determined by fundamental aerosol processes, which should lead to a more physically based simulation of aerosol direct and indirect radiative forcings. This study examines the global variation in particle size distribution simulated by twelve global aerosol microphysics models to quantify model diversity and to identify any common biases against observations. Evaluation against size distribution measurements from a new European network of aerosol supersites shows that the mean model agrees quite well with the observations at many sites on the annual mean, but there are some seasonal biases common to many sites. In particular, at many of these European sites, the accumulation mode number concentration is biased low during winter and Aitken mode concentrations tend to be overestimated in winter and underestimated in summer. At high northern latitudes, the models strongly underpredict Aitken and accumulation particle concentrations compared to the measurements, consistent with previous studies that have highlighted the poor performance of global aerosol models in the Arctic. In the marine boundary layer, the models capture the observed meridional variation in the size distribution, which is dominated by the Aitken mode at high latitudes, with an increasing concentration of accumulation particles with decreasing latitude. Considering vertical profiles, the models reproduce the observed peak in total particle concentrations in the upper troposphere due to new particle formation, although modelled peak concentrations tend to be biased high over Europe. Overall, the multi-model-mean dataset simulates the global variation of the particle size distribution with a good degree of skill, suggesting that most of the individual global aerosol microphysics models are performing well, although the large model diversity indicates that some models are in poor agreement with the observations. Further work is required to better constrain size-resolved primary and secondary particle

AEROCOM
microphysics
intercomparison

G. W. Mann et al.

Title Page

Abstract

Introduction

Conclusions

References

Tables

Figures



Back

Close

Full Screen / Esc

[Printer-friendly Version](#)

Interactive Discussion



number sources, and an improved understanding of nucleation and growth (e.g. the role of nitrate and secondary organics) will improve the fidelity of simulated particle size distributions.

1 Introduction

- 5 Atmospheric aerosol exerts a substantial influence on the Earth's climate both directly by scattering and absorbing short-wave solar and long-wave terrestrial radiation (e.g. Haywood and Boucher, 2000) and indirectly by affecting the evolution and optical properties of clouds (e.g. Lohmann and Feichter, 2005). There are also many other ways in which the atmospheric aerosol interacts with the Earth's climate system (e.g. Heintzenberg et al., 2012). Surface cooling induced by increases in aerosol abundance since the pre-industrial period may have partially offset the warming from increased greenhouse gases, but there is large uncertainty in the magnitude of aerosol radiative forcings, particularly in the indirect effects associated with changes in cloud properties (Forster et al., 2007). There is also a range of Earth System feedbacks associated with climate change induced changes in natural aerosol and precursor emissions (Carslaw et al., 2010) and these are expected to exert a strong influence on regional climate (Paasonen et al., 2013). There is a need for models to better quantify global aerosol properties and trends in order to reduce uncertainties in model projections of future changes in climate (Andreae et al., 2005) and over recent decades (Booth et al., 2012). To address 15 uncertainties in indirect forcings, it is particularly important to improve model representation of aerosol microphysical properties, such as particle number concentrations and size distributions.

Atmospheric aerosol particles have traditionally been separated into coarse and fine particles (diameters larger and smaller than about $2\text{ }\mu\text{m}$ respectively, e.g. Whitby, 1978), which broadly maps onto whether they were mechanically generated or formed 25 following growth from nanometre-sized nuclei. Aerosol particles are also classified as either primary (i.e. directly emitted), or secondary particles (formed in the atmosphere

[Title Page](#)

[Abstract](#)

[Introduction](#)

[Conclusions](#)

[References](#)

[Tables](#)

[Figures](#)

◀

▶

[Back](#)

[Close](#)

[Full Screen / Esc](#)

[Printer-friendly Version](#)

[Interactive Discussion](#)



from gas to particle nucleation). Fine particles are much more numerous than coarse particles (e.g. Raes et al., 2000) and consist of small primary particles (e.g. sub-micron sea-spray/dust and carbonaceous combustion aerosol) and also secondary particles, which initially form at nanometre sizes, but can grow by coagulation and condensation to large enough sizes to scatter visible radiation and activate into cloud droplets. Fine particles are further separated into Aitken and accumulation modes, based on observed number size distributions in a range of environments showing two distinct peaks, generally found in the 10 to 100 nm and 100 to 1000 nm dry diameter range (Raes et al., 2000). The larger peak occurs at particle sizes where both dry deposition and sedimentation are relatively inefficient, causing size distributions to evolve into a distinct “accumulation” mode. In remote marine regions, the two separate modes are caused by cloud processing, where the larger sub-set of fine particles activate to cloud droplets where they can grow larger following aqueous chemical reactions in non-precipitating clouds (Lelieveld and Heintzenberg, 1992; Hoppel et al., 1994). Near to particle sources, the Aitken peak often indicates freshly emitted primary particles. However, the Aitken size range also often contains secondary particles which have grown from an initial nucleation mode at around 1 to 3 nm (e.g. Kulmala et al., 2004).

Modelling the evolution of the particle size distribution is therefore rather complex, and requires an aerosol dynamics scheme whereby two or more moments (e.g. number and mass) are prognosed in several size classes. Models following this approach are called aerosol microphysics models, and can be broadly classified into two different types. Sectional schemes (Gelbard et al., 1980) discretize the particle size spectrum into multiple size bins whereas modal schemes (Whitby and McMurry, 1997) parameterize the variation of the size distribution within the nucleation, Aitken, accumulation and coarse ranges, with each mode usually approximated via a log-normal function in particle radius. In the 1990s, sectional aerosol microphysics schemes were incorporated into several regional air quality models (e.g. Jacobson, 1997a, Jacobson et al., 1997b, Lurmann et al., 1997) and have more recently become established in several global models (Adams and Seinfeld, 2002; Spracklen et al., 2005a, 2011; Yu and

[Title Page](#)

[Abstract](#)

[Introduction](#)

[Conclusions](#)

[References](#)

[Tables](#)

[Figures](#)

◀

▶

◀

▶

[Back](#)

[Close](#)

[Full Screen / Esc](#)

[Printer-friendly Version](#)

[Interactive Discussion](#)



Luo, 2009; Lee and Adams, 2010; Bergman et al., 2012). Two-moment modal aerosol microphysics schemes were similarly initially implemented into regional models (e.g. Binkowski and Shankar, 1995) and subsequently within several global models (Ghan et al., 2001a, b; Wilson et al., 2001; Stier et al., 2005; X. Liu et al., 2005, 2012; Bauer et al., 2008; Mann et al., 2010; Aan de Brugh et al., 2011; Zhang et al., 2012; Bellouin et al., 2013).

The international AeroCom initiative seeks to improve our understanding of global aerosol and associated radiative forcings and has provided a mechanism for co-ordinating efforts to evaluate and intercompare global aerosol models. The stated overall goals of AeroCom are to identify weaknesses in particular models and modelling aspects, and to assess uncertainties in simulated aerosol properties and radiative forcings (Kinne et al., 2006). The first phase of AeroCom aligned with the lead-up to the Intergovernmental Panel on Climate Change (IPCC) fourth climate assessment report (AR4), and resulted in several multi-model intercomparison papers documenting simulated aerosol optical properties (Kinne et al., 2006), aerosol lifecycles (Textor et al., 2006, 2007) and radiative forcings (Schulz et al., 2006; Penner et al., 2006). New observational constraints on simulated aerosol optical properties from satellite measurements and retrievals from the AERONET global network of sun photometers led to a reduced uncertainty range for aerosol direct forcings in AR4, which also caused a narrower uncertainty range in total anthropogenic radiative forcing (Haywood and Schulz, 2007).

Since AR4, many climate modelling centres have incorporated new aerosol modules that include size-resolved aerosol microphysics. This represents a major shift in model sophistication (Ghan and Schwarz, 2007) and improves upon previous “first generation” aerosol schemes in which aerosol optical properties and cloud droplet concentrations were based on the simulated mass of several externally mixed aerosol types, each assigned a prescribed size distribution. The microphysical aerosol schemes calculate and transport the number concentration and component mass in several size classes of particles and can also represent both external and internal mixtures. Separate trans-

[Title Page](#)

[Abstract](#)

[Introduction](#)

[Conclusions](#)

[References](#)

[Tables](#)

[Figures](#)

◀

▶

◀

▶

[Back](#)

[Close](#)

[Full Screen / Esc](#)

[Printer-friendly Version](#)

[Interactive Discussion](#)



port of size-resolved number and mass allows growth processes such as condensation and aqueous sulphate production to realistically conserve particle number while adding mass, and enables new particle formation and coagulation to provide explicit sources and sinks for particle number, which has been shown to be important in capturing

5 changes in aerosol in response to changing emissions (Bellouin et al., 2013). The microphysics models explicitly simulate the evolution of the particle size distribution, and use this to determine aerosol optical properties and cloud condensation nuclei concentrations. In so-doing, they represent aerosol interactions with clouds and radiation consistently with the underlying physics of the fundamental aerosol processes.

In the second phase of AeroCom (AeroCom-2), working groups have been established to examine different aspects of the global aerosol, with a new set of experiments defined (Schulz et al., 2009). Analysis of the AeroCom-2 experiments, and of the original set of experiments, have led to recent publications with multi-model comparisons of simulated direct forcings (Myhre et al., 2013), indirect effects (Quaas et al., 2009), black carbon (Koch et al., 2009; Schwarz et al., 2010; Samset et al., 2013), dust (Huneeus et al., 2011), vertical profiles (Koffi et al., 2012), radiative transfer (Stier et al., 2013; Randles et al., 2013) and organics (Tsigaridis et al., 2013). This paper reports initial findings from a working group to intercompare and evaluate twelve global aerosol microphysics models which participated in AeroCom-2. This initial study focuses on the particle size distribution, whose evolution is specifically simulated by these models, and has so far not specifically been considered in AeroCom publications. Note that we also plan a follow-up study to intercompare simulated CCN concentrations, and will use the globally varying size distribution fields derived here for offline calculations of cloud droplet number concentrations and first indirect radiative effects predicted by the global aerosol microphysics models.

The present paper has three key objectives. First, we aim to document the diversity of simulated particle number concentrations in several size ranges among the new generation of global aerosol microphysics models. Secondly, we derive datasets of multi-model mean particle concentrations that can be used as a reference for future

Title Page	
Abstract	Introduction
Conclusions	References
Tables	Figures
◀	▶
◀	▶
Back	Close
Full Screen / Esc	
Printer-friendly Version	
Interactive Discussion	



development and improvement of these models. Thirdly, we evaluate the multi-model mean (with associated diversity) against several benchmark observational datasets from ground station networks and compilations over multiple field campaigns. The chosen benchmark observational datasets have been selected to provide a climatological overview of the skill of the models covering both marine and a range of different continental environments, both at the surface and in the vertical profile. In carrying out these objectives, we aim to determine how well the models simulate aerosol microphysical properties and identify any generic weaknesses or gaps in scientific understanding.

2 Methodology

10 2.1 Particle size distribution metrics considered

Aerosol indirect radiative effects are driven by the sub-set of particles large enough to be activated to cloud droplets (so-called cloud condensation nuclei, CCN). Although the minimum size for activation can be just a few tens of nm for supersaturations of around 1.0 %, concurrent size distribution and CCN measurements for more moderate supersaturations of 0.2 to 0.5 % suggest that 50 to 100 nm is a reasonable value for the threshold CCN diameter (Kerminen et al., 2012). Aerosol microphysical processes such as nucleation, coagulation, condensation and cloud processing exert a strong control on the evolution of nucleation, Aitken and accumulation mode particle concentrations and are therefore very important in determining CCN concentrations.

20 In comparing and evaluating size distributions simulated by global aerosol micro-physics models, we will often consider integral size-resolved particle concentrations, which help summarise the comparisons and evaluation considering different sub-sets of particles. The number concentrations N_3 , N_{10} , N_{14} are integral concentrations of particles with dry diameters larger than 3 nm, 10 nm and 14 nm, and are often referred to as condensation nuclei (CN). The sizes refer to the typical thresholds of condensation particle counter (CPC) instruments, which we use to evaluate the total number of

particles simulated by the models across the full measurable particle size range. Not all of these particles are directly relevant to CCN, but they provide information about how well the models capture concentrations of secondary particles, which contribute a large fraction of CCN in many regions (e.g. Merikanto et al., 2009; Kerminen et al., 2012).

We also consider concentrations of particles larger than 30, 50 and 100 nm dry diameter (N_{30} , N_{50} and N_{100}). The N_{50} concentrations counts accumulation and coarse sized particles, and also part of the Aitken size range, with 50 nm representing the minimum size ammonium sulphate particles would activate at supersaturations of 0.42 % (a value typical for marine stratocumulus). The 30 nm dry diameter (N_{30}) represents a typical lower size limit for activation (0.9 % supersaturation) and 100 nm (N_{100}) represents an upper limit (0.14 % supersaturation). Aerosol optical properties are mainly controlled by particles larger than 100 nm, since they account for most of the light scattering at visible and longer wavelengths. None of these metrics are uniquely relevant to the aerosol effect on clouds and climate because the actual activation size depends on the particle chemical composition, cloud updraught velocity and the details of the full size distribution (e.g. Abdul-Razzak and Ghan, 2000; Nenes and Seinfeld, 2003). However, studies suggest (e.g. Dusek et al., 2006) that the particle number size distribution is the most important quantity in determining atmospheric CCN concentrations (Kerminen et al., 2012). The metrics therefore represent typical aerosol microphysical properties of relevance to climate and can easily and consistently be compared among models and with observations.

2.2 Description of model experiments

For the second phase of AeroCom co-ordinated experiments (Schulz et al., 2009), a new control present-day emissions simulation was defined (A2-CTRL-2006). A matching pre-industrial emissions double-call nudged run (A2-PRE-2006) was also requested for intercomparison of simulated direct aerosol forcings (see Myhre et al., 2013). To reduce inter-model differences, general circulation models (GCMs) were ad-

[Title Page](#)

[Abstract](#)

[Introduction](#)

[Conclusions](#)

[References](#)

[Tables](#)

[Figures](#)

[|◀](#)

[▶|](#)

[◀](#)

[▶](#)

[Back](#)

[Close](#)

[Full Screen / Esc](#)

[Printer-friendly Version](#)

[Interactive Discussion](#)



Seven of the models use modal aerosol schemes (GLOMAP-mode, ECHAM5-HAM2, EMAC, TM5, CAM5-MAM3, GISS-MATRIX and HadGEM-UKCA) and four use sectional schemes (GISS-TOMAS, GLOMAP-bin, ECHAM5-SALSA and GEOS-Chem-APM), whilst CanAM4-PAM is a hybrid approach combining bin and mode. Eleven of the 12 models use two-moment approaches whereby both the number and mass concentration in each size class are transported, allowing each size-class to have representative size which varies in time and space. The GEOS-Chem-APM model uses a single-moment approach, but has a large number of size classes to allow the size distribution to freely evolve in response to the processes.

Table 2 summarises the primary and secondary aerosol sources used in each model. Although the intention was for the models to use the same anthropogenic emissions from Diehl et al. (2012) for the year 2006, this was not achieved, with some submissions using the IPCC year 2000 emissions (Lamarque et al., 2010), and others using the AEROCOM first phase emissions (Dentener et al., 2006). In addition to these differences in emissions inventories, the models also used their own choice for the size and injection heights applied to primary emissions sources. Although recommendations for these emissions size assumptions were made by Dentener et al. (2006) for several source types based on measurements in the literature, there is a wide range of values used by the models. The assumed size has been shown to have a strong influence on simulated particle concentrations (Spracklen et al., 2010) and size distribution (Reddington et al., 2011), so we list these here for each model. Many of the models used prescribed oxidant fields in determining aerosol precursor oxidation, although five did have tropospheric chemistry schemes determining oxidant concentrations online in the simulation. A diversity of nucleation parameterizations was apparent across the models, with most including only binary homogeneous nucleation which produces particles only in the free troposphere. Only one of the models used an empirical boundary layer nucleation mechanism (e.g. Sihto et al., 2006) for their AEROCOM simulations, although some models simulate ternary or ion-induced/mediated nucleation which can generate particles efficiently in the boundary layer. The simulated burdens and surface

AEROCOM
microphysics
intercomparison

G. W. Mann et al.

Title Page

Abstract

Introduction

Conclusions

References

Tables

Figures

Tables Figures

Tables

Figures



Back

Close

Full Screen / Esc

Page 61 of 80

Interactive Discussion



AEROCOM microphysics intercomparison

G. W. Mann et al.

[Title Page](#)

[Abstract](#)

[Introduction](#)

[Conclusions](#)

[References](#)

[Tables](#)

[Figures](#)

[|◀](#)

[▶|](#)

[◀](#)

[▶](#)

[Close](#)

[Full Screen / Esc](#)

[Printer-friendly Version](#)

[Interactive Discussion](#)



size-resolved number concentrations from each model are also shown in Table 2 for reference.

Comparison of aerosol properties simulated by the same aerosol microphysics scheme implemented within different modelling frameworks, have been carried out for both sectional (Trivitayanurak et al., 2008) and modal (Zhang et al., 2010) modules, and have shown that predictions are sensitive to host model differences. We have therefore chosen not to try to discriminate the extent to which sectional schemes may outperform modal aerosol microphysics schemes, as we believe this would not be possible given the variety of host model frameworks used for the benchmark simulations.

2.3 Deriving comparable model size distributions

To compare particle size distributions between models of different complexity, the 3-D-varying number and size for each size class is required. The CanAM4-PAM and GEOS-Chem-APM models submitted datasets which had mapped their size classes onto a fixed size bin grid. Since all other models followed either two-moment modal or two-moment sectional size distribution approaches, a common methodology could be applied. First, the mean dry volume $V_{\text{dry},i}$ was calculated for each size class i summing over all present internally mixed aerosol components j (sulphate, sea-salt, black carbon (BC), organic matter, dust, nitrate or ammonium):

$$V_{\text{dry},i} = \sum_j \left(\frac{m_{ij} M_j}{N_a \rho_j} \right) \quad (1)$$

where m_{ij} is the number of molecules per particle of component j in mode i , ρ_j and M_j are the density and molar mass of component j and N_a is Avogadro's constant. The m_{ij} values were derived from each models' submitted number concentrations (n_i) and mass mixing ratios (q_{ij}) as

$$m_{ij} = \frac{M_{\text{da}}}{M_j} \frac{q_{ij}}{n_i} \frac{p}{k_B T} \quad (2)$$

where M_{da} is the molar mass of dry air, k_{B} is Boltzmann's constant and p and T are the ambient pressure and temperature. Once the mean dry volume for each size class was derived, the geometric (number) mean dry diameter \bar{D}_i was then calculated as:

$$\bar{D}_i = \left(\frac{6V_{\text{dry},i}}{\pi \exp(4.5 \log_e^2(\sigma_{g,i}))} \right)^{\frac{1}{3}} \quad (3)$$

- 5 where $\sigma_{g,i}$ is set to unity for sectional schemes and to their assumed constant values for the log-normal modes used by the modal schemes. Each modelling group provided a document explaining the mapping from tracer index to size class and aerosol component, together with their scheme's values for $\sigma_{g,i}$, ρ_j and M_j .

10 The monthly-mean number concentration N_i and size \bar{D}_i was then calculated for each size class on the 3-D grid. The vertical co-ordinate grid for each model was also constructed from the information provided.

15 Size-resolved number concentrations were then derived for particles larger than 3, 10, 14, 30, 50 and 100 nm by integrating the size distribution based on n_i , D_i and $\sigma_{g,i}$ in each size class. These threshold dry diameters (D_{thresh}) were chosen to facilitate comparison with the measurements described in Sect. 3.2. For modal schemes, partial integrals over each log-normal size class were computed using the error function. For sectional schemes, the calculation involved summing the number concentration in all size classes larger than the threshold size including a fractional contribution from bins with interface dry diameters that span D_{thresh} .

20 To enable size distributions to be assembled into a multi-model mean, each model's size distribution was calculated on a common size grid. For sectional models, the number size distribution $\frac{dN}{d\log_{10}(D)}$ was first constructed on the parent size grid:

$$\left\{ \frac{dN}{d\log_{10}(D)} \right\}_i = \log_e(10) \frac{N_i \bar{D}_i}{\Delta D_i} \quad (4)$$

Title Page	
Abstract	Introduction
Conclusions	References
Tables	Figures
◀	▶
◀	▶
Back	Close
Full Screen / Esc	
Printer-friendly Version	
Interactive Discussion	



where ΔD_i is from the parent model bin dry-diameter grid. These parent dry-diameter grid size distributions were then interpolated onto a common 50-bin grid D_k between 1 nm and 10 μm . For modal schemes, $\frac{\text{d}N}{\text{d}\log_{10}D}$ was calculated by evaluating the lognormal distribution on the common 50-bin grid:

$$\left\{ \frac{\text{d}N}{\text{d}\log_{10}(D)} \right\}_k = \log_e(10) \frac{N_i}{(2\pi)^{0.5} \log_e(\sigma_{g,i})} \exp \left\{ -\frac{(\log_e(D_k) - \log_e(\bar{D}_i))^2}{2 \log_e^2(\sigma_{g,i})} \right\} \quad (5)$$

Although calculating size-resolved number concentrations and size distributions from monthly-mean aerosol tracers does not account for higher temporal variations in mass to number ratios, the approach allows us to intercompare the full set of global aerosol microphysics models with a consistent methodology. To assemble the multi-model mean and diversity, each model quantity at the surface (BC, sulphate, N_{30} , N_{100}) was interpolated onto a 1° by 1° grid and zonal-means against latitude and height were interpolated onto a 1° by 100 m grid.

2.4 Definition of multi-model mean and diversity

In Sect. 3.1, we examine spatial distributions of multi-model mean and diversity over a “central” sub-set of the models, omitting models with aerosol properties outside a chosen range. Such central-model-mean fields provide a “best estimate” of the global distribution of aerosol properties and may also become useful as reference datasets against which to assess evolving model development. We follow the approach of Kinne et al. (2006) in using the central two-thirds (here 8 models) as the basis for the central model mean and diversity. When calculating the central-8 mean we take the geometric mean over the values for each model. Note that the assessment of which models are “central” is done locally, so the central mean will be over different models in different regions. As in Kinne et al. (2006), the diversity is presented as the ratio of the maximum and minimum values over those central two-thirds of models. This approach is useful

Title Page	
Abstract	Introduction
Conclusions	References
Tables	Figures
◀	▶
◀	▶
Back	Close
Full Screen / Esc	
Printer-friendly Version	
Interactive Discussion	

as it immediately gives the factor over which those central models range. It is important to note that we always refer to model diversity as the ratio of the central two-thirds maximum and minimum (rather than as an absolute quantity) to enable the diversity to be compared between clean and polluted regions. Finally, we note that multi-model di-

versity is not the same as the true model uncertainty. For example, the diversity may be low close to emissions sources if models use similar emissions inventories. Additional uncertainty will be caused by uncertainties in emissions (Lee et al., 2013a) which has not been accounted for here.

3 Results

10 3.1 Multi-model mean and diversity of aerosol properties

As a reference to help understand the mean and diversity of size-resolved number concentrations, we first examine simulated mass concentrations of sulphate and black carbon. We do not intercompare simulated particulate organic matter (POM) among the models as this is the subject of another AeroCom intercomparison paper (Tsi-

15 garidis et al., 2013). We also do not analyse simulated mass concentrations of dust and sea-salt as they are mainly from super- μm particles, whereas our focus is on sub- μm particles. Note however, that the size-resolved POM, dust and sea-salt masses in the models are included in the construction of the model size distributions, and hence their influence on size-resolved number concentration is accounted for.

20 3.1.1 Surface sulphate and black carbon

Sulphate is mostly a secondary aerosol species formed by oxidation of sulphur dioxide (SO_2). In marine regions SO_2 derives mainly from the oxidation of dimethyl sulphide (DMS), produced by phytoplankton, although SO_2 from continuously erupting volcanoes also has an important influence on aerosol properties (Andres and Kasg-
25 noc, 1998; Schmidt et al., 2012). In the present-day atmosphere, the dominant global



AEROCOM
microphysics
intercomparison

G. W. Mann et al.

source of sulphate is derived from anthropogenic SO₂ which greatly exceeds marine and volcanic SO₂ sources (e.g. Dentener et al., 2006). Figure 1a illustrates this strong anthropogenic influence, with the multi-model mean sulphate mass concentration highest over the main industrialised regions, with maximum surface annual means of 2 to 5 µg m⁻³ of sulphur over eastern China.

Black carbon (BC) mainly determines the aerosol absorption and is a primary aerosol mass species, being directly emitted from wildfires and anthropogenic fossil fuel and biofuel combustion sources. The global BC distribution in Fig. 1b reflects these source regions, and since the vast majority of BC is emitted from continental sources, marine concentrations are typically at least a factor of 10 lower than over the continents.

The central diversities of surface sulphate and BC mass (Fig. 1c and d) are generally lower in continental regions than in marine regions. For BC, which is almost entirely emitted in continental regions, this land-sea contrast in diversity is much greater. Since BC is a primary emitted species, the main cause of the diversity near to the sources is likely to be differences in emissions between the models, although boundary layer mixing and dry deposition may also play a role. Black carbon emissions are treated in all models based on prescribed emissions inventories, and Fig. 1d shows that the diversity in simulated BC concentrations is less than a factor of two in the main polluted regions.

In general, the diversity in surface BC (Fig. 1d) increases substantially with distance away from source, from a factor of about 3 in the main source regions to a factor of 4 to 6 in more remote marine regions, and to around a factor of 10 or more at high latitudes. These large diversities are consistent with the findings from Koch et al. (2009) who found the largest model BC diversity occurred in northern Eurasia and the remote Arctic and Schwarz et al. (2010) who showed that, over the remote Pacific, the ratio of the 75th to 25th percentiles was around a factor of 10 at the surface between 60° N and 60° S and a factor of 30 to 100 at higher latitudes. In these previous studies, the differences were attributed to both emissions and removal processes. The mapping of the diversity here suggests that differences in removal processes are the dominant source

Title Page	
Abstract	Introduction
Conclusions	References
Tables	Figures
◀	▶
◀	▶
Back	Close
Full Screen / Esc	
Printer-friendly Version	
Interactive Discussion	



of model BC diversity in remote regions (possibly in combination with approaches to ageing), because diversity is much lower in the main emissions regions. This finding agrees with recent studies (Vignati et al., 2010; Kipling et al., 2013) which have also found a strong influence of model treatment of scavenging on simulated BC in remote regions. Lee et al. (2013b) investigated the diversity in simulated BC from 7 models participating in the Atmospheric Chemistry and Climate Model Intercomparison Project (ACCMIP) and also found increasing diversity with increasing distance from source, with the standard deviation among simulated Arctic BC columns greater than their mean. In that study, only one of the chemistry-climate models was nudged to meteorological reanalysis data, while all models used the same emissions inventory, and the large diversity in simulated BC (a factor 3 for global column burdens) was found to be caused by differences in removal and transport.

The diversity in surface sulphate mass has regional variations that are not evident in BC. For example, there is much more diversity over the high-sulphate region in Europe than over the eastern United States (US). By contrast, the two regions have similar BC diversity at the surface, although the western US is more diverse in simulated BC, where wildfire emissions dominate. Figure 1c also shows that model diversity in simulated sulphate is much higher in northern Europe than in southern Europe. An important sulphate production mechanism is from aqueous oxidation of dissolved sulphur dioxide in cloud droplets (e.g. Barrie et al., 2001) via aqueous chemical reactions with dissolved hydrogen peroxide and ozone. In northern Europe, concentrations of hydrogen peroxide and ozone are much lower than in southern Europe (e.g. Berglen et al., 2004) and different treatments of chemistry, including some models' prescription of oxidant fields (see Table 2) could explain the higher sulphate diversity in northern Europe. The higher sulphate diversity in Northern Europe could also be explained by the expected increase with distance away from the source region, due to differences in the representation of removal processes. However, the BC diversity map does not show this maximum in Northern Europe, so the model treatment of sulphate production is the more likely cause. In their comprehensive analysis of aerosol microphysical un-

[Title Page](#)

[Abstract](#)

[Introduction](#)

[Conclusions](#)

[References](#)

[Tables](#)

[Figures](#)

◀

▶

◀

▶

[Back](#)

[Close](#)

[Full Screen / Esc](#)

[Printer-friendly Version](#)

[Interactive Discussion](#)



certainties, Lee et al. (2013a) also found that aqueous sulphate production was a major cause of uncertainty in simulated CCN at high northern latitudes.

3.1.2 Surface size-resolved particle concentrations

Figure 2 shows global maps of particle number concentrations with dry diameter larger than 30 nm (N_{30} , Fig. 2a) and 100 nm (N_{100} , Fig. 2b). In each gridbox, the central two-thirds of the model annual means was calculated, and the map shows the geometric mean over those 8 values. Surface N_{30} concentrations are highest in the main industrialised regions, due mainly to anthropogenic primary emissions. In eastern China, annual mean N_{30} reaches $10\,000\text{ cm}^{-3}$, and in India, central Europe and eastern USA there are large regions with annual-mean N_{30} above 2000 cm^{-3} . Regions with strong biomass burning emissions also have high annual mean N_{30} , with central Africa and South America in excess of 1000 cm^{-3} . In marine regions, N_{30} is much higher in the Northern Hemisphere than the Southern Hemisphere, exceeding 200 cm^{-3} everywhere between 30 and 60° N in the North Atlantic and North Pacific. By contrast, N_{30} is less than 200 cm^{-3} throughout the Southern Hemisphere marine boundary layer, falling below 100 cm^{-3} poleward of 60° S . It is interesting that, even in the Antarctic, annual mean N_{30} never falls below 50 cm^{-3} , whereas the annual means of N_{100} and the mass concentrations of sulphate and BC mass have steep meridional gradients towards the remote polar regions. This constant background N_{30} is likely due to a steady source of particles from nucleation in the free troposphere (e.g. Raes, 1995; Merikanto et al., 2009). The presence of this constant background source of potential CCN could be important for determining the baseline pre-industrial cloud droplet concentrations which has a strong influence on indirect forcing over the industrial period (e.g. Carslaw et al., 2013; Schmidt et al., 2012).

Surface N_{100} concentrations show a similar spatial distribution to N_{30} in continental regions, but with lower concentrations. However, in the outflow regions off the coast of East Asia and eastern USA, N_{100} decreases more rapidly away from the source than

[Title Page](#)[Abstract](#)[Introduction](#)[Conclusions](#)[References](#)[Tables](#)[Figures](#)[|◀](#)[▶|](#)[◀](#)[▶](#)[Back](#)[Close](#)[Full Screen / Esc](#)[Printer-friendly Version](#)[Interactive Discussion](#)

N_{30} which may reflect a lower proportion of particles in marine N_{100} than N_{30} . Another factor is that larger particles tend to be shorter-lived because they are more efficiently removed by nucleation scavenging. Only a weak local maximum in N_{100} is seen in the high sea-spray belt in the Southern Ocean between 40 and 55° S with N_{100} above 5 50 cm^{-3} , and N_{100} only falls below 10 cm^{-3} over continental Antarctica.

The diversity in the main anthropogenic emissions regions (Fig. 2c) is high for N_{30} (factor 2 to 5), whereas N_{100} is substantially lower (within a factor of 2, Fig. 2d) and follows a continental diversity pattern similar to BC (Fig. 1d). The high continental N_{30} diversity is partly due to differences in assumed size distribution for primary emissions sources in the different models (see Table 2). A smaller assumed size results in higher primary particle number emissions (for a given particle emission mass flux), and also affects simulated size-dependent processes such as gas to particle transfer and particle growth by coagulation and condensation. Different assumptions for the size distribution of primary emitted particles have been shown to strongly influence simulated particle number concentrations (Pierce and Adams, 2009; Spracklen et al., 2010). Reddington et al. (2011) examined the effect on model size distributions finding a stronger influence on simulated N_{30} than N_{100} in Europe where carbonaceous emissions are mostly from fossil fuel combustion sources. The size at which these primary particles are emitted also strongly affects how efficiently they are removed and also their cloud nucleating and optical properties. As seen in Table 2, although all the models represent new particle formation, most only include a binary nucleation mechanism such as Kulmala et al. (1998) or Vehkamaki et al. (2002). These parameterizations do not generate a significant number of new particles in the continental boundary layer (e.g. Spracklen et al., 2006; Merikanto et al., 2009; Yu et al., 2010), so the main particle number source in continental regions (near the surface) will tend to be from direct emission of primary particles (e.g. carbonaceous or sub-grid “primary sulphate” particles).

In remote marine regions, N_{30} has a relatively low diversity (a factor of 2), with higher values (factor 3 to 6) seen in regions where primary aerosol dominates the particle source, such as the sea-spray belt (40 to 55° S), and in biomass burning outflow regions

(Merikanto et al., 2009). Whereas N_{30} has much higher diversity in continental than marine regions, the reverse is true for N_{100} (Fig. 2d), which has a diversity generally within a factor of 2 in the anthropogenic source regions, although biomass burning regions are more diverse. Marine N_{100} is diverse among the central two-thirds, typically by around a factor 3 to 5, with even higher diversity near the equator.

The patterns of diversity in N_{30} and N_{100} can be explained by differences in the sources of the two size classes of particles. N_{30} in marine regions tends to be dominated by secondary particles which were nucleated in the free troposphere and subsequently entrained into the marine boundary layer (e.g. Raes, 1995; Clarke and Kapustin, 2002; Merikanto et al., 2009). Marine CCN concentrations have been shown (Spracklen et al., 2005b; Lee et al., 2013a) to be relatively insensitive to a factor of 10 change in the free tropospheric nucleation rate, due mainly to the negative feedback effect from coagulation being more effective at higher particle concentrations. In the main sea-spray region (40–50° S), the N_{30} diversity is much higher than in other marine regions, likely indicating differences in the way the models treat ultra-fine sea-spray, which is more diverse among the models than concentrations of entrained particles from the free troposphere. Observations from field campaigns (e.g. O'Dowd and Smith, 1993) and laboratory measurements (e.g. Martensson et al., 2003) have shown that sea-spray efficiently produces particles down to sub-100 nm dry-diameters and global model studies have shown that these ultrafine sea-spray particles contribute directly to CCN (Pierce and Adams, 2006) and also indirectly through their influence on the size distribution of marine sulphate aerosols (Gong and Barrie, 2003). The higher diversity in marine N_{100} (than N_{30}) may also be indicative of those particles being long-range transported or cloud-processed particles that have been shaped by several processes with a higher combined diversity.

3.1.3 Meridional and vertical distributions

In this section, we examine the modelled vertical and meridional distributions, considering zonal-means in each model as a function of latitude and altitude. Figure 3 shows



**AEROCOM
microphysics
intercomparison**

G. W. Mann et al.

[Title Page](#)[Abstract](#)[Introduction](#)[Conclusions](#)[References](#)[Tables](#)[Figures](#)[|◀](#)[▶|](#)[◀](#)[▶|](#)[Back](#)[Close](#)[Full Screen / Esc](#)[Printer-friendly Version](#)[Interactive Discussion](#)

[Title Page](#)[Abstract](#)[Introduction](#)[Conclusions](#)[References](#)[Tables](#)[Figures](#)[◀](#)[▶](#)[Back](#)[Close](#)[Full Screen / Esc](#)[Printer-friendly Version](#)[Interactive Discussion](#)

for BC since there is a substantial marine source of sulphate originating from DMS (mainly during summer).

The meridional and vertical distribution of N_{30} and N_{100} is shown in Fig. 4. The zonal-mean N_{100} distribution (Fig. 4b) is qualitatively similar to the BC distribution (Fig. 3b), but has a much slower decrease with increasing altitude, suggesting N_{100} is influenced by secondary particle sources in the free and upper troposphere. N_{30} has an even weaker vertical gradient, particularly in the Southern Hemisphere, consistent with N_{30} being more strongly influenced by secondary particles formed in the free troposphere than N_{100} .

The model diversity in N_{30} (Fig. 4c) is quite high at the surface due to differences in the size distribution of primary emissions. Above the boundary layer the N_{30} diversity is much lower as there is a mixture of nucleated and primary particles. It is interesting that for both N_{30} and N_{100} there is a maximum in model diversity at about 5 to 7 km in the tropics which could reflect differences in vertical transport and scavenging between the models.

3.2 Comparison with observations

Previous evaluation of multiple global aerosol models against observations (e.g. Kinne et al., 2006) has tended to focus on datasets with a wide spatial and temporal coverage, such as the AERONET sun photometer network (Holben et al., 1998) or satellite data (e.g. Tanre et al., 1997; Torres et al., 2002; Kahn et al., 1998). Although these datasets have given useful information on the global distribution of column aerosol optical properties, they provide only limited information on the particle size distribution. In-situ measurements of the particle size distribution have been made in numerous field campaigns and at monitoring sites over several decades, and several data compilations have been created that are useful for model evaluation.

Here, we evaluate the 12 global aerosol microphysics models against several such data compilations from airborne, ship-borne and land-based in-situ measurements. Global aerosol microphysics models are considerably more complex than mass-based

aerosol schemes with prescribed size distributions (see Sect. 2.2). As a consequence, intercomparing the size distributions simulated by different aerosol micro-physics schemes is a technically challenging exercise. Rather than providing a comprehensive evaluation of each model, the idea here is to assess the skill of the multi-model mean and isolate cases where the central models cannot account for the observations.
5 The datasets used are listed in Table 3 and are briefly described here:

– *Global Atmosphere Watch (GAW) sites*

The World Meteorological Organisation co-ordinates the GAW network of measurement stations (http://www.wmo.int/pages/prog/arep/gaw/gaw_home_en.html) to provide long-term monitoring of aerosol optical, physical and chemical properties. The first dataset we compare the aerosol microphysics models to are CPC measurements of total (size integrated) particle number concentration at 13 of the GAW sites. The measurements for these sites were downloaded from the World Data Centre for Aerosols (WDCA) database hosted by the EU Joint Research Centre, Ispra (<http://www.jrc.ec.europa.eu/data/parameters/datacnc.html>). Note that this database has now moved from JRC and is currently hosted at the Norwegian Institute for Air Research (NILU) within the wider EBAS database (<http://ebas.nilu.no/>).

As in Spracklen et al. (2010), we classify these 13 GAW sites into three types: free troposphere (FT): Jungfraujoch (JFJ), Mauna Loa (MLO), South Pole (SPO), marine boundary layer: Mace Head (MHT), Neumayer (NEU), Barrow (BRW), Samoa (SMO), Trinidad Head (THD), Cape Grim (CGR) and continental boundary layer: Southern Great Plains (SGP), Bondville (BND), Pallas (PAL) and Hohenpeissenberg (HOP). Many of these sites have several decades of data available which can be used to establish trends in aerosol concentration (e.g. Asmi et al., 2013). In this study, we compare to multi-annual means and standard deviations over the monthly-mean data over the number of years listed in Table 3.

Title Page

Abstract

Introduction

Conclusions

References

Tables

Figures

◀

▶

◀

▶

Back

Close

Full Screen / Esc

Printer-friendly Version

Interactive Discussion



Table 7 of Mann et al. (2010). The total number of years of data used, and the size thresholds for the CPC at each site are shown in Table 3. The four original NOAA baseline aerosol monitoring stations (SPO, BRW, SMO, MLO) have operated since the 1970s and are described by Bodhaine (1983). Further information on these and the other sites can be found in Collaud Coen et al. (2013) and Asmi et al. (2013).

5
– *European Supersites for Atmospheric Aerosol Research (EUSAAR)*

EUSAAR was a European project which established a co-ordinated network of 20 aerosol super-sites (Philippin et al., 2009) which are now supported by the ACTRIS initiative (Aerosols, Clouds, and Trace gases Research InfraStructure Network, <http://www.actris.net>). Each of the super-sites is equipped with differential or scanning mobility particle sizers (DMPS/SMPS) to measure particle size distributions following standardised protocols for instrument maintenance and measurement procedures (Wiedensohler et al., 2012). Asmi et al. (2011) compiled the EUSAAR measured size distribution datasets over 2008/09 and combined them with additional concurrent measurements from the German Ultrafine Aerosol Network (GUAN) which also had DMPS/SMPS instruments measuring sub- μm aerosol size distributions (Birmili et al., 2009). The general findings of the Asmi et al. (2011) study were that central European sites had strong unimodal size distributions with relatively low CCN variability, whereas Nordic and western European sites have lower concentrations, were more variable and often bimodal with distinct Aitken and accumulation modes. We compare the models to the climatological size distributions at each site from Asmi et al. (2011), and group them into five types; Nordic and Baltic: Aspreveten (ASP), Birkenes (BIR), Hyttiala (SMR), Pallas (PAL), Preila (PLA) and Vavihill (VHL), Central Europe: Bosel (BOS), Hohenpeissenberg (HPB), K-Puzsta (KPO), Kosetice (OBK), Melpitz (MPZ), Waldhof (WAL), Western Europe: Cabauw (CBW), Harwell (HWL), Mace Head (MHT), Mediterranean: Ispra (JRC), Finokalia (FKL) and Arctic: Zeppelin (ZEP).

10
15
20
25
13, 30841–30928, 2013

Title Page

Abstract

Introduction

Conclusions

References

Tables

Figures

◀

▶

◀

▶

Back

Close

Full Screen / Esc

Printer-friendly Version

Interactive Discussion



**AEROCOM
microphysics
intercomparison**

G. W. Mann et al.

[Title Page](#)[Abstract](#)[Introduction](#)[Conclusions](#)[References](#)[Tables](#)[Figures](#)[|◀](#)[▶|](#)[◀](#)[▶|](#)[Back](#)[Close](#)[Full Screen / Esc](#)[Printer-friendly Version](#)[Interactive Discussion](#)– *The Lindenberg Aerosol Characterization Experiment 1998 (LACE 98)*

The LACE 98 campaign (Petzold et al., 2002) took place over eastern Germany during summer 1998 with a range of airborne aerosol measurements made to characterise aerosol properties over central Europe. The aircraft instrumentation deployed in LACE 98 included three CPCs measuring total integral particle concentrations (with different lower size limits) and Passive Cavity Aerosol Spectrometer Probe (PCASP) measurements of the particle size distribution between 0.1 and 3 µm dry diameter. Further work to analyse and process these measurements led to median and 25th/75th percentile profiles of N_5 , N_{15} and N_{120} on a 1 km vertical grid (see Lauer et al., 2005) that have been used to evaluate size-resolved particle concentrations in the boundary layer and free troposphere, as simulated by global aerosol microphysics models. Note that when comparing to this dataset, each model's number concentrations are at ambient temperature and pressure to be consistent with the observed profiles.

– *30 yr of ship-borne aerosol measurements*

Marine boundary layer particle concentrations and number size distribution measurements have been compiled into a global climatological dataset (Heintzenberg et al., 2000). The dataset brings together measurements from several field campaigns in many regions including the Arctic (Heintzenberg and Leck, 1994; Covert et al., 1996), the central Pacific (Quinn et al., 1990, 1993, 1995, 1996), the North Atlantic (Van Dingenen et al., 1995; Leaitch et al., 1996; Raes et al., 1997) and the Southern Ocean and Antarctic (Jaenicke et al., 1992; Davison et al., 1996; Bates et al., 1998). The climatology has been used as an observational constraint for global model simulated Aitken and accumulation mode number, size and widths (e.g. Easter et al., 2004; Pierce and Adams, 2006; Spracklen et al., 2007; Trivitayanurak et al., 2008; Zhang et al., 2010; Mann et al., 2012). It would be highly desirable to repeat the valuable efforts of Heintzenberg et al. (2000), and produce a similar, updated marine climatology incorporating the wide range of aerosol microphysics measurement datasets made on cruises since 2000.

AEROCOM
microphysics
intercomparison

G. W. Mann et al.

- 10 yr of aircraft measurements over the Pacific and Southern Oceans

Data from numerous field campaigns have been compiled by Clarke and Kapustin (2002) to produce climatological profiles of ultrafine particle concentrations within latitude ranges 70° S to 20° S, 20° S to 20° N and 20° N to 70° N. The aircraft measurements very clearly show a distinct maximum in particle concentrations in the free and upper troposphere, which has been shown to provide an important source of CCN in marine regions (Merikanto et al., 2009). Note that when comparing to this dataset, each model's number concentrations are converted to standard temperature and pressure to be consistent with the observed profiles.

3.2.1 Total particle number concentrations at GAW sites

Figure 5 shows a scatter plot of modelled annual mean particle number concentrations against the multi-year annual mean from the observations at each site. The model values are geometric means over the central 8 model simulated concentrations of particles larger than the cut-off diameter used by the CPC at each measurement site (3, 10 or 14 nm, see Sect. 2.3 and Table 3). The vertical whiskers indicate the range over the central 8 models, whereas the horizontal whisker shows the standard deviation over the annual-means over the several years of measurements (see Table 3).

The central-model mean represents the spatial variation of the annual mean particle concentrations well with a Pearson correlation coefficient (R) of 0.96 and normalised mean bias (b) of -0.21 , and is within a factor 2 of the observations at all 13 sites. However, there are large differences in the model predictions. For example, at Pallas and Mace Head, the central model diversity is about a factor of 5. The three FT sites (Jungfraujoch, Mauna Loa and South Pole) have lower diversity but still it is around a factor 2 to 4. This large model diversity indicates that many of the models have considerable biases against the observations. However, at only 2 of the 13 sites (Southern Great Plains and Neumayer) does the central two-thirds range not span the multi-annual mean of the measurements. It is interesting that the central models have opposite bias at the two Antarctic sites, tending to be slightly biased high at the



South Pole site, but biased low at the coastal Neumayer site. Boundary layer nucleation events have been observed in a recent field campaign at Neumayer (R. Weller, personal communication, 2013) and have also been measured at the Finnish coastal Antarctic site Aboa (Asmi et al., 2010). The coastal N_{14} low bias could therefore be
 5 due to most models' nucleation parameterizations not forming new particles efficiently in the boundary layer. The other site with a low bias is Southern Great Plains in rural continental USA. As shown in Table 2, most of the model nucleation parameterizations do not generate particles efficiently in the boundary layer, and such boundary layer nucleation mechanisms have been shown to represent a substantial source of small
 10 particles in rural continental environments (e.g. Kulmala et al., 2004; Spracklen et al., 2006, 2008).

Annual cycles of total particle number at the GAW sites are shown in Figs. 6–8. Considering the free troposphere sites, Mauna Loa in Hawaii (19° N) has no significant seasonal variation (Fig. 6b), whereas Jungfraujoch (Fig. 6a) and South Pole (Fig. 6c) have clear seasonal cycles with summer total particle concentrations higher than in winter by factors of about 2 and 10 respectively. At South Pole, this seasonal cycle in N_{14} is likely driven by the strong seasonal variations in DMS seawater concentration and photochemistry although seasonal transport effects are also a likely contributor (Bodhaine et al., 1986). The central model mean captures the South Pole seasonal cycle in N_{14} very well ($R = 0.947$) albeit with a slight high bias ($b = 0.385$, as seen in Fig. 5), which worsens during winter. At Jungfraujoch, the seasonal cycle likely reflects stronger photochemistry during the summer, leading to higher gas phase H_2SO_4 concentrations or organic vapours which will tend to give higher nucleation rates at the site (Boulon et al., 2010). Increased pollution and transport from lower altitudes during the summer will also be an important influence. The models also show elevated N_{10} during summer at Jungfraujoch, although the central-8 mean model shows a moderate low bias ($b = -0.128$) during summer.

For the marine boundary layer GAW sites, the strong seasonal cycle at the Antarctic coastal site Neumayer (Fig. 7b) is well captured by the multi-model mean ($R = 0.92$),

Title Page	
stract	Introduction
clusions	References
ables	Figures
◀	▶
◀	▶
Back	Close
Full Screen / Esc	
rinter-friendly Version	
nteractive Discussion	



with the general low bias seen in Fig. 5 distributed evenly over the year ($b = -0.512$). However, at the Alaskan site Barrow, although the central-mean model compares fairly well with observations on the annual mean, the seasonal cycle is not well captured ($R = 0.22$), with the models highest in May when the observations show a local mini-

5 mum (Fig. 7c). Simulating Arctic aerosol is challenging because of the complex factors
 that lead to the formation of the Arctic haze observed in late winter and early spring
 (e.g. Quinn et al., 2002). The poor model performance is consistent with the findings
 of previous studies, which have highlighted the importance of seasonal variations in
 scavenging processes and local nucleation (Browse et al., 2012, 2013; Bougeois and
 10 Bey, 2011; Garrett et al., 2010; Huang et al., 2010; Korhonen et al., 2008a; J. Liu
 et al., 2011). At Mace Head (Fig. 7a), simulated particle concentrations are biased low
 ($b = -0.48$) as seen on the annual mean in Fig. 5, and the models also do not capture
 the observed concentration peaks in May and September ($R = 0.22$). At Cape Grim
 (Fig. 7f), the N_3 seasonal cycle (over all air masses) is fairly flat despite there being an
 15 established strong influence of DMS on the N_3 and CCN seasonal cycle from the
 marine air mass sector (e.g. Ayers and Gras, 1991; Korhonen et al., 2008b). At the other
 two sites: Samoa in the Pacific (Fig. 7d) and Trinidad Head on the US California coast
 (Fig. 7e), the observations show no clear seasonal cycle, but the models have highest
 concentrations in late summer at Trinidad Head, which is not seen in the observations.

At the continental boundary layer sites (except for Southern Great Plains), the central-8 model mean agrees well with the observations on the annual mean (Fig. 5). The weak seasonal N_{14} variation at Bondville (Fig. 8b) and Hohenpeissenberg (Fig. 8d) is also well captured by the central-8 model mean, although the models predict a peak at Hohenpeissenberg during March that is outside the observed multi-year mean plus or minus standard deviation (1995 to 2005). At Pallas (Fig. 8c), the observations show a strong seasonal variation, with monthly mean N_{10} concentrations around a factor 3 higher in spring and summer than in winter. The central-8 mean model particle concentration peaks in spring rather than summer, and the variation is weaker than in the observations (by about a factor 2). Spracklen et al. (2010) found that including a bound-

Title Page

Abstract Introduction

Conclusions References

Tables Figures

|◀ ▶|

◀ ▶

Back Close

Full Screen / Esc

Printer-friendly Version

Interactive Discussion



ary layer nucleation mechanism improves the seasonal variation in particle concentrations at continental sites, particularly at Pallas, although simulated concentrations tend to peak in spring whereas the observations show a peak in summer. Secondary organic aerosol has been shown to strongly influence new particle formation rates (e.g. Metzger et al., 2010) and Scott et al. (2013) examined the seasonal cycle in N_{30} at Hyttiala and Pallas, showing that the observed summertime peak in particle concentrations could be much better reproduced in their model when an organic-mediated nucleation parameterization was used.

3.2.2 Size-resolved number concentrations at EUSAAR/GUAN sites

Figure 9 compares the mean of the central two-thirds models with observed size-resolved particle concentrations at 17 low-altitude sites in the EUSAAR/GUAN network (Asmi et al., 2011). The seven sites above 900 m altitude were omitted as these tend to be affected by local factors, for example daily variations from polluted air masses from lower altitudes (Asmi et al., 2011), which is unlikely to be captured at the coarse resolution used in the global models.

Asmi et al. (2011) analysed the EUSAAR/GUAN observations, presenting percentiles of the size distributions and size-resolved number concentrations from the hourly measurements. However, since the model results are monthly means, i.e. an arithmetic mean over values at all timesteps, we compare here against an arithmetic-mean over the hourly observations (A. Asmi, personal communication, 2012). In the full size distribution comparisons (Figs. 14–16), the median observed values are also shown for reference (from Asmi et al., 2011). At most sites, the median and mean observed values are similar at sizes larger than 100 nm, but at Aitken mode sizes (10 to 100 nm), the median is much lower than the mean, suggesting it is temporally the more variable of the two modes.

Simulated N_{30} (Fig. 9a) is very diverse among the central 8 models at most of these European sites, more so than for N_{100} (Fig. 9c), more than 50 % of their mean at many sites. However, at the Arctic site Zeppelin N_{30} diversity is lower than for N_{100} , consis-

Title Page	
Abstract	Introduction
Conclusions	References
Tables	Figures
◀	▶
◀	▶
Back	Close
Full Screen / Esc	
Printer-friendly Version	
Interactive Discussion	



tent with the spatial distribution in diversity seen in Fig. 2. Despite this large model diversity however, as seen for the comparisons to the CPC measurements (Fig. 5), the central two-thirds model mean generally compares quite well with the observations on the annual-mean, with $R = 0.795, 0.801, 0.784$ and $b = -0.192, -0.228, -0.359$ for 5 N_{30}, N_{50}, N_{100} respectively over the full set of sites. At all sites, except Ispra (which is strongly influenced by local pollution sources) and the Arctic site Zeppelin, the central mean is within a factor of 2 of the observations for all three size ranges on the annual mean. Aside from Zeppelin, the N_{100} particle concentrations have lower diversity and also generally compare better with the measurements than N_{30} and N_{50} . This suggests 10 that CCN concentrations (which can be approximated by N_{50}) are more diverse among the models than are aerosol optical properties (which are mainly influenced by particles larger than 100 nm). It is noticeable however that Ispra and Preila have a stronger low bias at N_{100} than N_{30} .

Simulated size-resolved number concentrations across the full annual cycle are compared 15 to the EUSAAR/GUAN observations in Fig. 10 (Nordic and Baltic sites), Fig. 11 (western European, Mediterranean and Arctic sites) and Fig. 12 (central European sites). Figure 13 summarises these seasonal cycle comparisons in terms of the winter and summer bias (model divided by observed) for each site.

From Fig. 9 we have seen that, on that annual mean, at the Nordic and Baltic sites, 20 the central two-thirds mean is in good agreement with the observations for N_{30}, N_{50} and especially N_{100} . However, the seasonal cycle is less well captured at these sites (Fig. 10). In particular, for several of the sites, the central-8 mean model N_{30} is mostly biased high during the winter (see also Fig. 13) and biased low during the summer. This discrepancy is similar to the total particle concentration comparison at Pallas (Fig. 8c), 25 with the multi-model value having a fairly flat seasonal variation whereas the observations show concentrations at least a factor 2 higher in summer than winter. By contrast, the central-8 model mean captures the seasonal variation in N_{100} much better. A possible explanation for the poor seasonal variation of small CCN is that only one of the models includes boundary layer nucleation, which generates small CCN effectively dur-

Title Page	
Abstract	Introduction
Conclusions	References
Tables	Figures
◀	▶
◀	▶
Back	Close
Full Screen / Esc	
Printer-friendly Version	
Interactive Discussion	



AEROCOM
microphysics
intercomparison

G. W. Mann et al.

[Title Page](#)

[Abstract](#)

[Introduction](#)

[Conclusions](#)

[References](#)

[Tables](#)

[Figures](#)

◀

▶

[Back](#)

[Close](#)

[Full Screen / Esc](#)

[Printer-friendly Version](#)

[Interactive Discussion](#)



[Title Page](#)[Abstract](#)[Introduction](#)[Conclusions](#)[References](#)[Tables](#)[Figures](#)[|◀](#)[▶|](#)[◀](#)[▶|](#)[Back](#)[Close](#)[Full Screen / Esc](#)[Printer-friendly Version](#)[Interactive Discussion](#)

contrast, new particle formation episodes are much less frequent at Harwell, occurring on only around 5 % of observation days (Charron et al., 2007).

We saw in Fig. 9 that the models underpredicts particle concentrations at Ispra for all three size ranges. In Fig. 11e, it is clear the low bias at this site is apparent throughout the year, with the accumulation mode (represented by N_{100}) particularly strongly under-estimated $b = -0.736$, with even the highest of the central models being too low. Very high N_{100} is observed during winter, likely reflecting local boundary layer trapping of nearly pollution sources adjacent to steep orography, which will tend to be poorly represented at the coarse resolution of the global models. Another source of error in N_{100} could be that most of the models do not represent nitrate aerosol, which efficiently partitions into the particle phase during the colder winter months (e.g. Adams et al., 1999), although this alone is unlikely to explain such a large N_{100} discrepancy.

At the five central European sites (Fig. 12), the central-8 model mean N_{30} compares quite well to the observations over the annual cycle. However, at several of these central European sites (Bosel, Kosecice, Melpitz, Waldhof), the observed N_{30} shows a local maximum in April or May that is not seen in the models. For N_{100} there is quite good agreement at the five sites during summer, with a weak low bias, but there is a much larger low bias during winter at many of the sites, as was also seen at Ispra.

An overview of the summer and winter N_{30} , N_{50} and N_{100} biases against the measurements is shown in Fig. 13. As seen for the annual mean comparisons, aside from Ispra and Zeppelin, modelled N_{100} is generally in good agreement with the observations during summer. During winter however, modelled N_{100} is biased low at many sites, which could indicate missing number sources at those sizes or insufficient growth from smaller sizes. Aquila et al. (2011) evaluated a global aerosol microphysics model against a different set of European size distribution measurements (Van Dingenen et al., 2004) and also found that, in the accumulation mode, number concentrations had a strong low bias during winter but were in much better agreement during summer. Nitric acid partitions into the particle phase during winter forming an important component of the sub-micron particle mass (e.g. Adams et al., 1999), and this may account

Title Page	
Abstract	Introduction
Conclusions	References
Tables	Figures
	
	
Back	Close
Full Screen / Esc	
Printer-friendly Version	
Interactive Discussion	



for some of the missing mass. Tsigaridis et al. (2013) find a general underprediction of wintertime organics which will also contribute to this model accumulation mode low bias.

For N_{30} the agreement is also reasonable, however the median model often has a high bias during winter and a low bias during summer. This was also seen for the total particle concentrations comparison for Pallas (see Fig. 8c) with a flat seasonal cycle in the models whereas the observations showed greatly enhanced concentrations during the summer. A factor that could explain some of this bias is that many of the models may have used too small particle size leading to a high bias in particle number emissions derived from the emitted mass flux. This would lead to too many particles in the Aitken sizes and too few in the accumulation mode, which would also be consistent with the N_{30} and N_{100} biases seen at many of these continental sites. There is clear need for improved understanding of primary and secondary particle sources, and better constraints for model assumptions for the size of primary emitted particles. Future studies are needed to carry out more detailed comparisons of the model size distributions to the new measurements from the EUSAAR/GUAN supersites. For example these could examine probability density functions over high temporal resolution model and observed datasets and apply cluster analysis techniques (Beddows et al., 2009), such as are already being applied to the EUSAAR/GUAN sites (Beddows et al., 2013).

3.2.3 Sub-micron size distributions at European surface sites

Figures 14–16 compare simulated particle size distributions against the SMPS/DMPS measurements at the EUSAAR and GUAN sites. The upper panels (a–f) are for summer with the lower panels (g–l) showing winter. Model size distributions are derived from the different complexity models following the methodology described in Sect. 2.3. When comparing the multi-model size distribution to the measurements, one should compare the red solid line (central model geometric mean) to the black solid line, which shows the arithmetic mean over the hourly observations for that month. The observed

**AEROCOM
microphysics
intercomparison**

G. W. Mann et al.

[Title Page](#)[Abstract](#)[Introduction](#)[Conclusions](#)[References](#)[Tables](#)[Figures](#)[|◀](#)[▶|](#)[◀](#)[▶|](#)[Back](#)[Close](#)[Full Screen / Esc](#)[Printer-friendly Version](#)[Interactive Discussion](#)

pares quite well with, if anything, a slight high bias at some sites. However, the wintertime accumulation mode low bias seen in the Nordic and Baltic sites is very evident here.

At Harwell during summer (Fig. 16b) the multi-model mean compares very well with the observations across the entire size range, but in winter (Fig. 16h) there is much too little number (and mass) in the accumulation mode and too much number below 100 nm dry radius. At Mace Head and Cabauw, during summer (Fig. 16a and c), although there is good agreement above 100 nm dry radius, there is a strong underestimation of number in the Aitken mode size range (10 to 100 nm) at both sites, although the size of the Aitken mode peak is well represented. The summertime Aitken low-bias, and the high variability in the Aitken size range (difference between the solid and dashed black lines in Fig. 16a), would be consistent with biogenic nucleation events occurring during summer as observed frequently at the coastal Mace Head site (e.g. O'Dowd et al., 2007). At Cabauw however, the median and mean size distribution are similar across the size range suggesting a more uniform particle source is missing or underestimated in the models. Also, considering Fig. 16g and i, whereas Mace Head compares better in the Aitken mode during summer, the Cabauw Aitken mode low bias is present in both seasons, suggesting the cause of the model-observation discrepancy may be different between the two sites. As noted in the discussion around Fig. 11b, new particle formation events are rather infrequent at Harwell (Charron et al., 2007), and the better agreement there is consistent with such secondary particle production not being well captured by the models.

At the Arctic site Zeppelin, during summer (Fig. 16f), the multi-model mean has a low bias across the size range, although the models do capture the observed shape of the size distribution with the Aitken mode peak being around a factor 2 higher than the accumulation mode peak. During winter however (Fig. 16l), the observations suggest the Aitken peak is a factor 10 higher than the accumulation mode peak, whereas the multi-model mean predicts the ratio less than 2. The observed 5th to 95th percentile range suggests very high observed particle concentrations are sporadically observed

13, 30841–30928, 2013

ACPD

[Title Page](#)

[Abstract](#)

[Introduction](#)

[Conclusions](#)

[References](#)

[Tables](#)

[Figures](#)

◀

▶

◀

▶

[Back](#)

[Close](#)

[Full Screen / Esc](#)

[Printer-friendly Version](#)

[Interactive Discussion](#)



Title Page	
Abstract	Introduction
Conclusions	References
Tables	Figures
◀	▶
◀	▶
Back	Close
Full Screen / Esc	
Printer-friendly Version	
Interactive Discussion	



at around 10 nm dry radius, which indicates a strong local nucleation or ultrafine particle source, that none of the central models capture.

At the Mediterranean site Finokalia, the multi-model mean compares well with the observations in both summer and winter (Fig. 16d and j). The good agreement in the accumulation mode at this site is consistent with the model wintertime accumulation mode low bias seen at other sites being caused by semi-volatile organics or nitrate since the warmer conditions at Finokalia will mean these species will tend not to partition into the particle phase there. At Ispra (Fig. 16e and k), the previously identified very strong wintertime accumulation mode low bias is clearly evident, likely due to boundary layer trapping of local pollution sources. During the summer there is a more moderate low bias across both Aitken and accumulation sized particles.

3.2.4 Vertical profile of size distribution over Europe

Figure 17 compares the models against a compilation of aircraft measurements of size-resolved particle concentrations from the LACE 98 field campaign (Petzold et al., 2002). The measurements comprise vertical profiles of N_5 and N_{15} from two CPCs, and N_{120} from integrating the size distribution measured by the PCASP instrument (as presented by Lauer et al., 2005). For this comparison, the model data for August was interpolated to 14.0° N, 52.1° E, the mid-point of the relatively small region of the flights (13.5–14.5° N, 51.5–52.7° E, Lauer et al., 2005). The model vertical profiles were then interpolated onto a common pressure grid between 950 and 220 hPa.

The modelled accumulation mode particle concentrations (represented here by N_{120}) capture the vertical profile well (Fig. 17c), although throughout the lowest few kilometres there is a considerable low bias. For particle concentrations at the smallest sizes (N_5 and N_{15}), the central two-thirds model mean is also biased low in the boundary layer, but is biased high (around a factor of 5) in the free and upper troposphere. Within the boundary layer the observations show a sharp increase in N_5 and N_{15} towards the surface that is not captured by the central models, likely due to nucleation being underestimated. The observations also suggest only a weak peak in N_5 in the up-

per troposphere, with maximum concentrations of about 800 cm^{-3} , whereas the models predict a strong peak with a central-8 mean and range of about 3000 cm^{-3} and $900\text{--}10\,000\text{ cm}^{-3}$. In contrast, as we show below, aircraft measurements of N_3 over the northern Pacific (Clarke and Kapustin, 2002) show much higher concentrations in the upper troposphere, up to 5000 cm^{-3} . A recently compiled database (Heintzenberg et al., 2011) of over 10 yr (1997 to 2008) of CPC measurements in the upper troposphere aboard two commercial aircraft as part of the CARIBIC project (e.g. Hermann et al., 2003) shows generally lower concentrations over Europe than over the North Atlantic, potentially due to the higher condensation sink over continents leading to lower ambient sulphuric acid vapour concentrations and thus lower nucleation rates.

3.2.5 Marine boundary layer size distributions

Marine boundary layer (MBL) particle size distribution measurements from Heintzenberg et al. (2000), based on 30 yr of field campaigns, are shown for the Southern Hemisphere (Fig. 18) and Northern Hemisphere (Fig. 19). The data compilation is based on 15° latitude band averaging of ship-borne measurements using Differential Mobility or Aerodynamic Particle Sizers (DMPS/APS). To derive equivalent size distributions from the models, the number concentration and representative dry diameters for each model's size class were averaged over marine gridboxes in each of the 15° latitude bands.

The observations show that accumulation mode number concentrations are approximately symmetric across the equator, while Aitken mode particle concentrations are around a factor two higher in the Southern Hemisphere than in the Northern Hemisphere. The measurements also show that typical sizes of both Aitken and accumulation modes are around 25 % larger in the Northern Hemisphere, implying a factor 2 higher particle volume concentration, approximately matching observations of sulphate mass.

Title Page	
Abstract	Introduction
Conclusions	References
Tables	Figures
◀	▶
◀	▶
Back	Close
Full Screen / Esc	
Printer-friendly Version	
Interactive Discussion	



In the Southern Hemisphere (Fig. 18), the central models capture the general variation of the boundary layer size distribution, with the observed minimum between the Aitken and accumulation modes (e.g. Hoppel et al., 1994) at around the right size, although peak concentrations are biased low by about a factor 2 south of 30° S. The shift 5 in the Aitken-accumulation mode $dN/d\log_{10} r$ ratio is also well captured, with the Aitken mode peak stronger than the accumulation mode south of 30° S, whereas these two size distribution peaks are of similar magnitude between 30° S and the equator.

In the Northern Hemisphere (Fig. 19), the multi-model mean size distribution is rather flat, which likely indicates that the models do not agree on the position of the Hoppel 10 gap rather than the models predicting a flat size distribution across the Aitken and accumulation size ranges. However, the weak bias in the central model simulated peaks seen in the Southern Hemisphere is not present here, although the Aitken mode peak is too high in mid-latitudes. The general shift in the Aitken-accumulation $dN/d\log_{10} r$ ratio is again well captured, with the two peaks approximately equal at low latitudes 15 and the Aitken mode peak much stronger at high latitudes. However, in contrast to the Southern Hemisphere, the observations suggest that the accumulation mode peak is much stronger than the Aitken mode between 30° N and 45° N, likely due to anthropogenic influences, which the central model size distributions do not capture.

Figure 20 compares the meridional variation of N_{10} (Fig. 20a) and particle concentrations 20 in the Aitken (Fig. 20b) and accumulation (Fig. 20c) size ranges. The comparisons show that although the general variation of the size distributions is well captured, the hemispheric asymmetry in N_{10} and Aitken mode concentrations is not reproduced by any of the models.

A general finding across all the models is that Aitken mode particle concentrations 25 are underpredicted in Southern Hemisphere mid-latitudes and overpredicted in Northern Hemisphere mid-latitudes. The Southern Hemisphere low bias in Aitken mode particle concentrations has also been found in multi-model comparisons of sectional (Trivitayanurak et al., 2008) and modal schemes (Zhang et al., 2010). Pierce and Adams (2006) found the bias was much reduced by using sea-spray source functions which

[Title Page](#)

[Abstract](#)

[Introduction](#)

[Conclusions](#)

[References](#)

[Tables](#)

[Figures](#)

◀

▶

◀

▶

[Back](#)

[Close](#)

[Full Screen / Esc](#)

[Printer-friendly Version](#)

[Interactive Discussion](#)



capture the observed efficient emission at ultrafine particle sizes (e.g. Martensson et al., 2003; Clarke et al., 2006). The meridional variation of accumulation mode concentrations is better captured with good agreement in the Northern Hemisphere, but a low bias in the Southern Hemisphere mid and high latitudes. As noted by Spracklen et al. (2007), it is also important to realise that most of the Southern Hemisphere cruise measurements in the Heintzenberg et al. (2000) observation climatology were taken during the summer. So some of the apparent low-bias in Aitken and accumulation mode concentrations there may just be reflecting a sampling bias with higher concentrations tending to be observed and modelled (not shown) during the summer.

3.2.6 Vertical profile of particle concentrations in marine regions

Figure 21 compares vertical profiles of total particle concentrations (N_3) over the Pacific and Southern Oceans against profiles compiled from aircraft measurements (Clarke and Kapustin, 2002). These measurements were produced from ultrafine condensation particle counter (u-CPC) measurements over several field campaigns (GLOBE-2: May 1990, ACE-1: November 1995, PEM-Tropics A: September 1996 and PEM-Tropics-B: March 1999), and compiled as three separate climatological profiles for the Southern Hemisphere (70° S– 20° S), tropical regions (20° S– 20° N) and the Northern Hemisphere (20° N– 70° N).

In the free and upper troposphere, over all three marine regions, the central models capture the vertical N_3 profile very well, with relatively small inter-model diversity. This agreement is in contrast to Europe, where the models overestimate particle concentrations (Fig. 17). The observed maximum in particle concentrations (which reflects the balance between particle production via nucleation and loss via coagulation) is captured very well by the central-8 model mean in the northern and Southern Hemisphere regions, although it is biased slightly low in the tropics. The central-8 model mean captures boundary layer N_3 concentrations well in the tropics and particularly the Northern Hemisphere, although there is a slight low bias compared to the aircraft measurements in the Southern Hemisphere. Considering the full model range, one model is showing

a factor 20–50 too high particle concentrations, which could indicate too high sulphuric acid vapour concentrations or that the nucleation parameterization is producing particles much too efficiently. The lowest model has N_3 a factor 10 too low throughout the free troposphere. Since N_3 is dominated by secondary particles from new particle formation, the low bias could be due to an aerosol surface area high bias in the free troposphere, which would give too low simulated sulphuric acid concentrations and nucleation rates. Lee et al. (2011) considered the effect on simulated CCN concentrations of co-varying eight parameters in a global aerosol microphysics model, showing that in the European free troposphere, simulated CCN concentrations are highly sensitive to parameters associated with the treatment of nucleation scavenging.

4 Conclusions

We have carried out the largest ever intercomparison of model simulated size distributions among the new generation of global aerosol microphysics models. Twelve global microphysics models have participated in the co-ordinated experiments within the AeroCom multi-model intercomparison initiative. We have derived benchmark multi-model datasets based around the mean of the central two-thirds of these models which provides a best estimate of global variation of the sub-micrometre particle size distribution, critical for understanding aerosol-climate interactions. These multi-model datasets will also serve as a useful reference to assist in model development.

An assessment of the diversity of the central two-thirds of models has identified regions where the models agree and disagree in terms of their predictions of size-resolved particle concentrations and mass concentrations of black carbon and sulphate. The different patterns of diversity can be explained by dominating aerosol processes and their associated uncertainty. In regions of strong anthropogenic emissions, the diversity of simulated number concentrations of particles larger than 30 nm dry-diameter (N_{30}) is very high (factor 2 to 6), while the diversities of N_{100} (factor 1.5 to 2) and of sulphate and black carbon mass concentrations (factor 1.2 to 3) are lower.

AEROCOM
microphysics
intercomparison

G. W. Mann et al.

[Title Page](#)

[Abstract](#)

[Introduction](#)

[Conclusions](#)

[References](#)

[Tables](#)

[Figures](#)

◀

▶

◀

▶

[Back](#)

[Close](#)

[Full Screen / Esc](#)

[Printer-friendly Version](#)

[Interactive Discussion](#)



The high N_{30} diversity in emissions regions is most likely due to inter-model differences in the size distribution assumed for primary emitted particles, which is a key parameter in need of better observational constraint. In remote marine regions, the pattern of size-resolved diversity is opposite to polluted regions, with N_{30} diversity (factor 1.5 to

5 2) much lower than for N_{100} (factor 2 to 5), sulphate (factor 2 to 4) and black carbon (factor 5 to 15). The relatively low N_{30} diversity in remote environments suggests that current global aerosol microphysics models are fairly consistent in their simulations of “natural” background CCN concentrations. Model diversity is highest in polar regions, where N_{30} diversity reaches a factor 2 to 7 and N_{100} diversity a factor 6 to 20.

10 Although there is large model diversity, the central models in general capture well the global variation of the size distribution. For example, the mean of the central two-thirds models agrees very well with observed total particle concentrations at Global Atmosphere Watch sites on the annual-mean. Exceptions are poor agreement at the Arctic site Barrow, and moderate high biases at South Pole and moderate low biases

15 at Samoa, Mace Head, Neumayer and Southern Great Plains. For this central two-thirds mean, agreement is reasonable against particle size distributions over Europe, aside from the Arctic site Zeppelin, and Ispra, which is strongly affected by nearby pollution sources and steep orography, features not expected to be well captured by the global models. However, there are some important biases common among the models

20 at many of the EUSAAR/GUAN sites. For example there is a strong underprediction of accumulation mode particle concentrations during winter, which is likely due to inadequately constrained particle number sources (both primary and secondary) or underprediction of growth due to a general underprediction of wintertime mass sources of nitrate and secondary organic aerosol, or both. The results also show that model

25 Aitken mode concentrations are too high during winter and too low during summer, which may reflect an underprediction of particle growth (to larger sizes) in winter and an underprediction of nucleation events in the summer.

The central models capture well the general meridional variation of size distribution in marine regions, with number concentrations at high latitudes mainly in the Aitken mode,

[Title Page](#)

[Abstract](#)

[Introduction](#)

[Conclusions](#)

[References](#)

[Tables](#)

[Figures](#)

◀

▶

◀

▶

[Back](#)

[Close](#)

[Full Screen / Esc](#)

[Printer-friendly Version](#)

[Interactive Discussion](#)



whereas the Aitken and accumulation modes have similar number concentrations in the tropics and mid-latitudes. However, for total particle concentrations (larger than 10 nm) there is a general overestimation in the Northern Hemisphere mid-latitudes and a low bias in the Southern Hemisphere mid-latitudes. The Southern Ocean low bias in total and Aitken particle number concentrations may be due to the models not adequately capturing the observed emission of sea-spray at sub-100 nm sizes (e.g. O'Dowd and Smith, 1993; Clarke et al., 2006; Pierce and Adams, 2006).

The global aerosol microphysics models capture very well the observed peak in ultra-fine condensation nuclei concentrations in the upper troposphere, which is caused by efficient new particle formation in that region. In continental regions there is a tendency to overpredict particle concentrations which could indicate a deficiency in nucleation parameterizations or in the simulated condensation sink.

Overall, the multi-model-mean dataset constructed in this study has been shown to have reasonable skill in simulating global particle size distributions, albeit with some important biases in some locations and seasons. The incorporation of aerosol micro-physics schemes into climate models has the potential to represent a significant step forward in the fidelity of simulated aerosol radiative forcings. The findings here indicate suggests that most of these global aerosol microphysics models are performing quite well in terms of global variation of the size distribution. Further work to compare the models against size distribution observations at higher temporal resolution is required to better characterise primary and secondary particle sources. Greater understanding of the role of secondary organic aerosol and other components (e.g. nitrate) in affecting nucleation and particle growth in the boundary layer is also required.

Acknowledgements. GWM and KSC received funding from the National Centre for Atmospheric Science, one of the UK Natural Environment Research Council (NERC) research centres. NERC research grants funded DVS (NE/G015015/1) and LAL (NE/G006172/1), while DAR was funded via an NERC Doctoral Training Grant. MTW and GWM received EU funding from the European Research Council (ERC) under Seventh Framework Programme (FP7) consortium projects MACC and MACC-II (grant agreements 218793 and 283576 respectively). CLR, KJP and KSC also received ERC FP7 funding under the PEGASOS Integrated Project (grant 30883

[Title Page](#)

[Abstract](#)

[Introduction](#)

[Conclusions](#)

[References](#)

[Tables](#)

[Figures](#)

[◀](#)

[▶](#)

[◀](#)

[▶](#)

[Back](#)

[Close](#)

[Full Screen / Esc](#)

[Printer-friendly Version](#)

[Interactive Discussion](#)



AEROCOM
microphysics
intercomparison

G. W. Mann et al.

Title Page

Abstract

Introduction

Conclusions

References

Tables

Figures

◀

▶

◀

▶

Back Close

Full Screen / Esc

Printer-friendly Version

Interactive Discussion



agreement 265148). NB, MD, CEJ were supported as part the UK Integrated Climate Programme funded by the Department for Energy and Climate Change (DECC) and Department for Environment Food and Rural Affairs – DECC/Defra (GA01101). SJG, RCE and XL were supported by the US Department of Energy (DOE) Scientific Discoveries through Advanced Computing program. The Pacific Northwest National Laboratory (PNNL) is operated for the DOE by Battelle Memorial Institute under contract DE-AC06-76RLO 1830. SEB and KT were supported by the NASA Modeling, Analysis and Prediction Program (NASA NNX09AK66G) with supercomputing resourced via the NASA High-End Computing (HEC) Program through the NASA Center for Climate Simulation (NCCS) at Goddard Space Flight Center. PS has been supported by the NERC project AEROS (NE/G006148/1) and received EU funding from the European Research Council (ERC) under FP7 grant agreement FP7-280025. KJP, HT and JL received funding from the ERC (grant agreement 226144). KZ was supported by funding from the Max Planck Society. Simulations with ECHAM5-HAM2 were performed at the German Climate Computing Center (Deutsches Klimarechenzentrum GmbH, DKRZ). KvS was supported by the Canadian Foundation for Climate and Atmospheric Sciences (CFCAS) and Environment Canada. AS acknowledges financial support from the Flemish agency for Innovation by Science and Technology (IWT) through the Climate and Air Quality Modelling for Policy Support (CLIMAQS) project. FY and GL were supported by NASA under grant NNX11AQ72G and NSF under grant 0942106. The EUSAAR network of aerosol supersites were established with EU funding from the Research Infrastructure Action under the FP6 Structuring the European Research Area Programme, Contract RII3-CT-2006-026140. Data for the Aspvreten and Zeppelin sites was provided by the Atmospheric Science Unit, Department of Applied Env. Sci, Stockholm University with financial support from the Swedish Environmental Protection Agency. The Harwell station is operated with financial support from the UK Department for Environment, Food and Rural Affairs. The Mace Head station received support from several Irish Government Agencies including the EPA, Met Eireann, and Department of the Environment. SGJ and CDOD would like to acknowledge the support of the European Union, through various projects within the 5th, 6th and 7th Framework programmes. JH gratefully acknowledges financial support from the German Ministry of Education and Science (AFO 2000 program) and from the European Commission's DGXII Environment RTD 4th, 5th, 6th and 7th framework programs. Airborne data provided by A. Clarke, University of Hawaii, represent about two decades of approximately equal support from the NSF-Atmospheric Chemistry Program and the NASA-Earth Science Division.

**AEROCOM
microphysics
intercomparison**

G. W. Mann et al.

- Aan de Brugh, J. M. J., Schaap, M., Vignati, E., Dentener, F., Kahnert, M., Sofiev, M., Huijnen, V., and Krol, M. C.: The European aerosol budget in 2006, *Atmos. Chem. Phys.*, 11, 1117–1139, doi:10.5194/acp-11-1117-2011, 2011.
- 5 Abdul-Razzak, J. and Ghan, S. J.: A parameterization of aerosol activation: 2. Multiple aerosol types, *J. Geophys. Res.*, 105, 6837–6844, 2000.
- Adams, P. J. and Seinfeld, J. H.: Predicting global aerosol size distributions in general circulation models, *J. Geophys. Res.*, 107, 4370, doi:10.1029/2001JD001010, 2002.
- 10 Adams, P. J., Seinfeld, J. H., and Koch, D. M.: Global concentrations of tropospheric sulfate, nitrate and ammonium aerosol simulated in a general circulation model, *J. Geophys. Res.*, 104, 13791–13823, 1999.
- Andreae, M. O., Jones, C. D., and Cox, P. M.: Strong present-day aerosol cooling implies a hot future, *Nature*, 435, 1187–1190, doi:10.1038/nature03671, 2005.
- 15 Andres, R. J. and Kasgnoc, A. D.: A time-averaged inventory of subaerial volcanic sulfur emissions, *J. Geophys. Res.*, 103, 25251–25261, 1998.
- Aquila, V., Hendricks, J., Lauer, A., Riemer, N., Vogel, H., Baumgardner, D., Minikin, A., Petzold, A., Schwarz, J. P., Spackman, J. R., Weinzierl, B., Righi, M., and Dall'Amico, M.: MADE-in: a new aerosol microphysics submodel for global simulation of insoluble particles and their mixing state, *Geosci. Model Dev.*, 4, 325–355, doi:10.5194/gmd-4-325-2011, 2011.
- 20 Asmi, A., Wiedensohler, A., Laj, P., Fjaeraa, A.-M., Sellegrí, K., Birmili, W., Weingartner, E., Baltensperger, U., Zdimal, V., Zikova, N., Putaud, J.-P., Marinoni, A., Tunved, P., Hansson, H.-C., Fiebig, M., Kivekäs, N., Lihavainen, H., Asmi, E., Ulevicius, V., Aalto, P. P., Swietlicki, E., Kristensson, A., Mihalopoulos, N., Kalivitis, N., Kalapov, I., Kiss, G., de Leeuw, G., Henzing, B., Harrison, R. M., Beddows, D., O'Dowd, C., Jennings, S. G., Flentje, H., Weinhold, K., Meinhardt, F., Ries, L., and Kulmala, M.: Number size distributions and seasonality of submicron particles in Europe 2008–2009, *Atmos. Chem. Phys.*, 11, 5505–5538, doi:10.5194/acp-11-5505-2011, 2011.
- 25 Asmi, A., Collaud Coen, M., Ogren, J. A., Andrews, E., Sheridan, P., Jefferson, A., Weingartner, E., Baltensperger, U., Bukowiecki, N., Lihavainen, H., Kivekäs, N., Asmi, E., Aalto, P. P., Kulmala, M., Wiedensohler, A., Birmili, W., Hamed, A., O'Dowd, C., G Jennings, S., Weller, R., Flentje, H., Fjaeraa, A. M., Fiebig, M., Myhre, C. L., Hallar, A. G., Swietlicki, E., Kristensson, A., and Laj, P.: Aerosol decadal trends – Part 2: In-situ aerosol

Title Page	
Abstract	Introduction
Conclusions	References
Tables	Figures
◀	▶
◀	▶
Back	Close
Full Screen / Esc	
Printer-friendly Version	
Interactive Discussion	



particle number concentrations at GAW and ACTRIS stations, *Atmos. Chem. Phys.*, 13, 895–916, doi:10.5194/acp-13-895-2013, 2013.

Asmi, E., Frey, A., Virkkula, A., Ehn, M., Manninen, H. E., Timonen, H., Tolonen-Kivimäki, O., Aurela, M., Hillamo, R., and Kulmala, M.: Hygroscopicity and chemical composition of Antarctic sub-micrometre aerosol particles and observations of new particle formation, *Atmos. Chem. Phys.*, 10, 4253–4271, doi:10.5194/acp-10-4253-2010, 2010.

Ayers, G. and Gras, J.: Seasonal relationship between cloud condensation nuclei and aerosol methanesulphonate in marine air, *Nature*, 353, 834–835, 1991.

Barrie, L. A., Yi, Y., Leaitch, W. R., Lohmann, U., Kasibhatla, P., Roelofs, G.-J., Wilson, J., McGovern, F., Benkovitz, C., Melieres, M. A., Law, K., Prospero, J., Kristz, M., Bergmann, D., Bridgeman, C., Chin, M., Christensen, J., Easter, R., Feichter, J., Land, C., Jeuken, A., Kjellstrom, E., Koch, D., and Rasch, P.: A comparison of large-scale atmospheric sulphate aerosol models (COSAM): overview and highlights, *Tellus B*, 53, 615–645, 2001.

Bates, T. S., Kapustin, V. N., Quinn, P. K., Covert, D. S., Coffman, D. J., Mari, C., Durkee, P. A., De Bruyn, W. J., and Saltzman, E. S.: Processes controlling the distribution of aerosol particles in the lower marine boundary layer during the First Aerosol Characterization Experiment (ACE 1), *J. Geophys. Res.*, 103, 16369–16383, 1998

Bauer, S. E., Wright, D. L., Koch, D., Lewis, E. R., McGraw, R., Chang, L.-S., Schwartz, S. E., and Ruedy, R.: MATRIX (Multiconfiguration Aerosol TRacker of mIXing state): an aerosol microphysical module for global atmospheric models, *Atmos. Chem. Phys.*, 8, 6003–6035, doi:10.5194/acp-8-6003-2008, 2008.

Beddows, D. C. S., Dall’Osto, M., and Harrison, R. M.: Cluster analysis of rural, urban and curbside atmospheric particle size data, *Environ. Sci. Technol.*, 43, 4694–4700, 2009.

Beddows, D. C. S., Dall’Osto, M., Harrison, R. M., Kulmala, M., Asmi, A., Wiedensohler, A., Laj, P., Fjaeraa, A.-M., Sellegrí, K., Birmili, W., Bukowiecki, N., Weingartner, E., Baltensperger, U., Zdimal, V., Zikova, N., Putaud, J.-P., Marinoni, A., Tunved, P., Hansson, H.-C., Fiebig, M., Kivekas, A., Swietlicki, E., Lihavainen, H., Asmi, E., Ulevicius, V., Aalto, P. P., Mihalopoulos, N., Kalivitis, N., Kalapov, I., Kiss, G., de Leeuw, G., Henzing, B., O’Dowd, C., D., Jennings, S. G., Flentje, H., Meinhardt, F., Ries, L., Denier van der Gon, H. A. C., and Visschedijk, A. J. H.: Variations in tropospheric submicron particle size distributions across the European continent 2008–2009, *in press.*, *Atmos. Chem. Phys. Discuss.*, 2013.

Bellouin, N., Mann, G. W., Woodhouse, M. T., Johnson, C., Carslaw, K. S., and Dalvi, M.: Impact of the modal aerosol scheme GLOMAP-mode on aerosol forcing in the Hadley Centre Global

**AEROCOM
microphysics
intercomparison**

G. W. Mann et al.

[Title Page](#)[Abstract](#)[Introduction](#)[Conclusions](#)[References](#)[Tables](#)[Figures](#)[◀](#)[▶](#)[◀](#)[▶](#)[Back](#)[Close](#)[Full Screen / Esc](#)[Printer-friendly Version](#)[Interactive Discussion](#)

- Berglen, T. F., Berntsen, T. K., Isaksen, I. S. A., and Sundet, J. K.: A global model of the coupled
5 sulfur/oxidant chemistry in the troposphere: the sulfur cycle, *J. Geophys. Res.*, 109, D19310,
doi:10.1029/2003JD003948, 2004.
- Bergman, T., Kerminen, V.-M., Korhonen, H., Lehtinen, K. J., Makkonen, R., Arola, A., Mielonen,
10 T., Romakkaniemi, S., Kulmala, M., and Kokkola, H.: Evaluation of the sectional aerosol
microphysics module SALSA implementation in ECHAM5-HAM aerosol-climate
model, *Geosci. Model Dev.*, 5, 845–868, doi:10.5194/gmd-5-845-2012, 2012.
- Binkowski, F. S., and Shankar, U.: The Regional Particulate Matter Model: 1. Model description
15 and preliminary results, *J. Geophys. Res.*, 100, 26191–26209, 1995.
- Birmili, W., Weinhold, K., Nordmann, S., Wiedensohler, A., Spindler, G., Müller, K., Her-
15 rmann, H., Gnauk, T., Pitz, M., Cyrys, J., Flentje, H., Nickel, C., Kulhbusch, T., Lschau, G.,
Haase, D., Meinhardt, F., Schwerin, A., Ries, L., and Wirtz, K.: Atmospheric aerosol measure-
ments in the German Ultrafine Aerosol Network (GUAN), Part 1: Soot and particle number
distributions, *Gefahrst. Reinhalt. L.*, 69, 137–145, 2009.
- Bodhaine, B. A.: Aerosol measurements at four background sites, *J. Geophys. Res.*, 88, 10753–
10768, 1983.
- Bodhaine, B. A., Deluisi, J. J., Harris, J. M., Houmere, P., and Bauman, S.: Aerosol measure-
20 ments at the South Pole, *Tellus B*, 38, 223–235, 1986.
- Booth, B., B. B., Dunstone, N. J., Halloran, P. R., Andrews, T., and Bellouin, N.: Aerosols im-
plicated as a prime driver of twentieth-century North Atlantic climate variability, *Nature*, 484,
228–232, 2012.
- Boulon, J., Sellegrí, K., Venzac, H., Picard, D., Weingartner, E., Wehrle, G., Collaud Coen, M.,
25 Bütkofer, R., Flückiger, E., Baltensperger, U., and Laj, P.: New particle formation and ultrafine
charged aerosol climatology at a high altitude site in the Alps (Jungfraujoch, 3580 m a.s.l.,
Switzerland), *Atmos. Chem. Phys.*, 10, 9333–9349, doi:10.5194/acp-10-9333-2010, 2010.
- Bourgeois, Q. and Bey, I.: Pollution transport efficiency toward the Arctic: sensitiv-
30 ity to aerosol scavenging and source regions, *J. Geophys. Res.*, 116, D08213,
doi:10.1029/2010JD015096, 2011.
- Browse, J., Carslaw, K. S., Arnold, S. R., Pringle, K., and Boucher, O.: The scavenging pro-
cesses controlling the seasonal cycle in Arctic sulphate and black carbon aerosol, *Atmos.
Chem. Phys.*, 12, 6775–6798, doi:10.5194/acp-12-6775-2012, 2012.

AEROCOM
microphysics
intercomparison

G. W. Mann et al.

Title Page

Abstract

Introduction

Conclusions

References

Tables

Figures

◀

▶

Back

Close

Full Screen / Esc

Printer-friendly Version

Interactive Discussion



**AEROCOM
microphysics
intercomparison**

G. W. Mann et al.

[Title Page](#)

[Abstract](#)

[Introduction](#)

[Conclusions](#)

[References](#)

[Tables](#)

[Figures](#)

◀

▶

[Back](#)

[Close](#)

[Full Screen / Esc](#)

[Printer-friendly Version](#)

[Interactive Discussion](#)



Browse, J., Carslaw, K. S., Mann, G. W., Birch, C. E., Arnold, S. R., and Leck, C.: The complex response of Arctic cloud condensation nuclei to sea-ice retreat, *Atmos. Chem. Phys. Discuss.*, 13, 17087–17121, doi:10.5194/acpd-13-17087-2013, 2013.

Carslaw, K. S., Boucher, O., Spracklen, D. V., Mann, G. W., Rae, J. G. L., Woodward, S., and Kulmala, M.: A review of natural aerosol interactions and feedbacks within the Earth system, *Atmos. Chem. Phys.*, 10, 1701–1737, doi:10.5194/acp-10-1701-2010, 2010.

Carslaw, K. S., Lee, L. A., Reddington, C. L., Pringle, K. J., Rap, A., Forster, P. M., Mann, G. W., Spracklen, D. V., Woodhouse, M. T., Regayre, L. A. and Pierce, J. R.: Large contribution of natural aerosols to uncertainty in indirect forcing, *Nature*, 503, 67–71, doi:10.1038/nature12674, 2013.

Charron, A., Birmili, W., and Harrison, R. M.: Factors influencing new particle formation at the rural site, Harwell, UK, *J. Geophys. Res.*, 112, D14210, doi:10.1029/2007JD008425, 2007.

Clarke, A. D. and Kapustin, V. N.: A Pacific aerosol survey, Part 1: a decade of data on particle production, transport, evolution and mixing in the troposphere, *J. Atmos. Sci.*, 59, 363–382, 2002.

Clarke, A. D., Owens, S. R., and Zhou, J.: An ultrafine sea-salt flux from breaking waves: implications for CCN in the remote marine atmosphere, *J. Geophys. Res.*, 111, D06202, doi:10.1029/2005JD006565, 2006.

Collaud Coen, M., Andrews, E., Asmi, A., Baltensperger, U., Bukowiecki, N., Day, D., Fiebig, M., Fjaeraa, A. M., Flentje, H., Hyvärinen, A., Jefferson, A., Jennings, S. G., Kouvarakis, G., Lihavainen, H., Lund Myhre, C., Malm, W. C., Mihopoulos, N., Molenar, J. V., O'Dowd, C., Ogren, J. A., Schichtel, B. A., Sheridan, P., Virkkula, A., Weingartner, E., Weller, R., and Laj, P.: Aerosol decadal trends – Part 1: In-situ optical measurements at GAW and IMPROVE stations, *Atmos. Chem. Phys.*, 13, 869–894, doi:10.5194/acp-13-869-2013, 2013.

Covert, D. S., Wiedensohler, A., Aalto, P., Heintzenberg, J., McMurry, P. H., and Leck, C.: Aerosol number size distributions from 3 to 500 nm diameter in the arctic marine boundary layer during summer and autumn, *Tellus B*, 48, 197–212, 1996.

Davison, B., O'Dowd, C., D., Hewitt, C. N., Smith, M. H., Harrison, R. M., Peel, D. A., Wolf, E., Mulvaney, R., Schwikowski, M., and Baltensperger, U.: Dimethyl sulfide and its oxidation products in the atmosphere of the Atlantic and Southern Oceans, *Atmos. Environ.*, 30, 1895–1906, 1996.

Dentener, F., Kinne, S., Bond, T., Boucher, O., Cofala, J., Generoso, S., Ginoux, P., Gong, S., Hoelzemann, J. J., Ito, A., Marelli, L., Penner, J. E., Putaud, J.-P., Textor, C., Schulz, M.,

AEROCOM
microphysics
intercomparison

G. W. Mann et al.

van der Werf, G. R., and Wilson, J.: Emissions of primary aerosol and precursor gases in the years 2000 and 1750 prescribed data-sets for AeroCom, *Atmos. Chem. Phys.*, 6, 4321–4344, doi:10.5194/acp-6-4321-2006, 2006.

Diehl, T., Heil, A., Chin, M., Pan, X., Streets, D., Schultz, M., and Kinne, S.: Anthropogenic, biomass burning, and volcanic emissions of black carbon, organic carbon, and SO₂ from 1980 to 2010 for hindcast model experiments, *Atmos. Chem. Phys. Discuss.*, 12, 24895–24954, doi:10.5194/acpd-12-24895-2012, 2012.

Dusek, U., Frank, G. P. Hildebrandt, L., Curtius, J., Schneider, J., Walter, S., Chand, D., Drewnick, F., Hings, S., Jung, D., Borrmann, S., and Andreae, M. O.: Size matters more than chemistry for cloud-nucleating ability of aerosol particles, *Science*, 312, 1375–1378, 2006.

Easter, R. C., Ghan, S. J., Zhang, Y., Saylor, R. D., Chapman, E. G., Laulainen, N. S., Abdul-Razzak, H., Leung, R., Bian, X., and Zaveri, R. A.: MIRAGE: model description and evaluation of aerosols and trace gases, *J. Geophys. Res.*, 109, D20210, doi:10.1029/2004JD004571, 2004

Forster, P., Ramaswamy, V., Artaxo, P., Berntsen, T., Betts, R., Fahey, D. W., Haywood, J., Lean, J., Lowe, D. C., Myhre, G., Nganga, J., Prinn, R., Raga, G., Schulz, M., and Van Dorland, R.: Climate Change 2007: the Physical Science Basis, in: Changes in Atmospheric Constituents and in Radiative Forcing, Contribution of Working Group I to the Fourth Assessment Report of the Intergovernmental Panel on Climate Change, Cambridge University Press, Cambridge, New York, 129–234, 2007.

Garrett, T. J., Zhao, C., and Novelli, P. C.: Assessing the relative contributions of transport efficiency and scavenging to seasonal variability in Arctic aerosol, *Tellus B*, 62, 190–196, 2010.

25 Gelbard, F., Tambour, Y., and Seinfeld, J. H.: Sectional representations for simulating aerosol dynamics, *J. Colloid Interf. Sci.*, 76, 541–556, 1980.

Ghan, S. J. and Schwartz, S. E.: Aerosol properties and processes: a path from field and laboratory measurements to global climate models, *B. Am. Meteorol. Soc.*, 88, 1059–1083, 2007.

³⁰ Ghan, S. J., Laulainen, N., Easter, R. C., Wagener, R., Nemesure, S., Chapman, E., Zhang, Y., and Leung, R.: Evaluation of aerosol direct radiative forcing in MIRAGE, *J. Geophys. Res.*, 106, 5295–5316, 2001a.

Title Page

Abstract

Introduction

Conclusions

References

Tables

Figures

1

1

Back

[Close](#)

Full Screen / Esc

[Printer-friendly Version](#)

Interactive Discussion



- Ghan, S. J., Easter, R. C., Hudson, J., and Breon, F.-M.: Evaluation of aerosol indirect radiative forcing in MIRAGE, *J. Geophys. Res.*, 106, 5317–5334, 2001b.
- Gong, S.-L. and Barrie, L.: Simulating the impact of sea salt on global nss sulphate aerosols, *J. Geophys. Res.*, 108, 4516, doi:10.1029/2002JD003181, 2003.
- 5 Haywood, J. and Boucher, O.: Estimates of the direct and indirect radiative forcing due to tropospheric aerosols – a review, *Rev. Geophys.*, 38, 513–543, 2000.
- Haywood, J. and Schulz, M.: Causes of the reduction in uncertainty in the anthropogenic radiative forcing of climate between IPCC (2001) and IPCC (2007), *Geophys. Res. Lett.*, 34, L20701, doi:10.1029/2007GL030749, 2007.
- 10 Heintzenberg, J.: The aerosol-cloud-climate conundrum, *Int. J. Global Warm.*, 4, 219–241, 2012.
- Heintzenberg, J. and Leck, C.: Seasonal variation of the atmospheric aerosol near the top of the marine boundary layer over Spitsbergen related to the Arctic sulphur cycle, *Tellus B*, 46, 52–67, 1994.
- 15 Heintzenberg, J., Covert, D. C., and Van Dingenen, R.: Size distribution and chemical composition of marine aerosols: a compilation and review, *Tellus B*, 52, 1104–1122, 2000.
- Heintzenberg, J., Hermann, M., Weigelt, A., Clarke, A., Kapustin, V., Anderson, B., Thornhill, K., van Velthoven, P., Zahn, A., and Brenninkmeijer, C.: Near-global aerosol mapping in the upper troposphere and lowermost stratosphere with data from the CARIBIC project, *Tellus B*, 63, 875–890, 2011.
- 20 Hermann, M., Heintzenberg, J., Wiedensohler, A., Zahn, A., Heinrich, G., and Brenninkmeijer, C. A. M.: Meridional distributions of aerosol particle number concentrations in the upper troposphere and lower stratosphere obtained by Civil Aircraft for Regular Investigation of the Atmosphere Based on an Instrument Container (CARIBIC) flights, *J. Geophys. Res.*, 108, 4114, doi:10.1029/2001JD001077, 2003.
- 25 Holben, B., Eck, T., Slutsker, I., Tanre, D., Buis, J., Vermote, E., Reagan, J., Kaufman, Y., Nakajima, T., Lavenau, F., Jankowiak, I., and Smirnov, A.: AERONET, a federated instrument network and data-archive for aerosol characterization, *Remote Sens. Environ.*, 66, 1–66, 1998.
- 30 Hoppel, W. A., Frick, G. M., Fitzgerald, J. W., and Larson, R. E.: Marine boundary-layer measurements of new particle formation and the effects nonprecipitating clouds have on aerosol size distribution, *J. Geophys. Res.*, 99, 14443–14459, 1994.

Title Page	
Abstract	Introduction
Conclusions	References
Tables	Figures
◀	▶
◀	▶
Back	Close
Full Screen / Esc	
Printer-friendly Version	
Interactive Discussion	



- Huang, L., Gong, S. L., Jia, C. Q., and Lavoue, D.: Importance of deposition processes in simulating the seasonality of the Arctic black carbon aerosol, *J. Geophys. Res.*, 115, D17207, doi:10.1029/2009JD013478, 2010.
- Huneeus, N., Schulz, M., Balkanski, Y., Griesfeller, J., Prospero, J., Kinne, S., Bauer, S., Boucher, O., Chin, M., Dentener, F., Diehl, T., Easter, R. C., Fillmore, D., Ghan, S. J., Ginoux, P., Grini, A., Horowitz, L., Koch, D., Krol, M. C., Landing, W., Liu, X., Mahowald, N., Miller, R., Morcrette, J.-J., Myhre, G., Penner, J., Perlitz, J., Stier, P., Takemura, T., and Zender, C. S.: Global dust model intercomparison in AeroCom phase I, *Atmos. Chem. Phys.*, 11, 7781–7816, doi:10.5194/acp-11-7781-2011, 2011.
- Jacobson, M. Z.: Development and application of a new air pollution modeling system – II. Aerosol module structure and design, *Atmos. Environ.*, 31, 131–144, 1997a.
- Jacobson, M. Z.: Development and application of a new air pollution modeling system – III, *Atmos. Environ.*, 31, 587–608, 1997b
- Jaecker-Voirol, A. and Mirabel, P.: Heteromolecular nucleation in the sulfuric acid-water system, *Atmos. Environ.*, 23, 2053–2057, 1989.
- Jaenicke, R., Dreiling, V., Lehmann, E., Koutsenoguii, P. K., and Stingl, J.: Condensation nuclei at the German Antarctic Station “Georg von Neumayer”, *Tellus B*, 44, 311–317, 1992.
- Jeuken, A., Siegmund, P., Heijboer, L., Feichter, J., and Bengtsson, L.: On the Potential of assimilating meteorological analyses in a global climate model for the purposes of model validation, *J. Geophys. Res.*, 101, 16939–16950, 1996.
- Jones, A., Roberts, D. L., Woodage, M. J., and Johnson, C. E.: Indirect sulfate aerosol forcing in a climate model with an interactive sulfur cycle, *J. Geophys. Res.*, 106, 20293–20310, 2001.
- Kahn, R., Banerjee, P., McDonald, D., and Diner, D. J.: Sensitivity of multi-angle imaging to aerosol optical depth and to pure particle size distribution and composition over ocean, *J. Geophys. Res.*, 103, 32195–32213, 1998.
- Kazil, J., Stier, P., Zhang, K., Quaas, J., Kinne, S., O'Donnell, D., Rast, S., Esch, M., Ferрrachat, S., Lohmann, U., and Feichter, J.: Aerosol nucleation and its role for clouds and Earth's radiative forcing in the aerosol-climate model ECHAM5-HAM, *Atmos. Chem. Phys.*, 10, 10733–10752, doi:10.5194/acp-10-10733-2010, 2010.
- Kerminen, V.-M., Paramonov, M., Anttila, T., Riipinen, I., Fountoukis, C., Korhonen, H., Asmi, E., Laakso, L., Lihavainen, H., Swietlicki, E., Svenningsson, B., Asmi, A., Pandis, S. N., Kulmala, M., and Petäjä, T.: Cloud condensation nuclei production associated with atmospheric

[Title Page](#)

[Abstract](#)

[Introduction](#)

[Conclusions](#)

[References](#)

[Tables](#)

[Figures](#)

[◀](#)

[▶](#)

[◀](#)

[▶](#)

[Back](#)

[Close](#)

[Full Screen / Esc](#)

[Printer-friendly Version](#)

[Interactive Discussion](#)



5 Kinne, S., Schulz, M., Textor, C., Guibert, S., Balkanski, Y., Bauer, S. E., Berntsen, T., Berglen, T. F., Boucher, O., Chin, M., Collins, W., Dentener, F., Diehl, T., Easter, R. C., Feichter, J., Fillmore, D., Ghan, S. J., Ginoux, P., Gong, S., Grini, A., Hendricks, J., Herzog, M., Horowitz, L., Isaksen, I., Iversen, T., Kirkevåg, A., Kloster, S., Koch, D., Kristjansson, J. E., Krol, M., Lauer, A., Lamarque, J. F., Lesins, G., Liu, X., Lohmann, U., Montanaro, V., Myhre, G., Penner, J., Pitari, G., Reddy, S., Seland, O., Stier, P., Takemura, T., and Tie, X.: An AeroCom initial assessment – optical properties in aerosol component modules of global models, *Atmos. Chem. Phys.*, 6, 1815–1834, doi:10.5194/acp-6-1815-2006, 2006.

10 Kipling, Z., Stier, P., Schwarz, J. P., Perring, A. E., Spackman, J. R., Mann, G. W., Johnson, C. E., and Telford, P. J.: Constraints on aerosol processes in climate models from vertically-resolved aircraft observations of black carbon, *Atmos. Chem. Phys.*, 13, 5969–5986, doi:10.5194/acp-13-5969-2013, 2013.

15 Koch, D., Schulz, M., Kinne, S., McNaughton, C., Spackman, J. R., Balkanski, Y., Bauer, S., Berntsen, T., Bond, T. C., Boucher, O., Chin, M., Clarke, A., De Luca, N., Dentener, F., Diehl, T., Dubovik, O., Easter, R. C., Fahey, D. W., Feichter, J., Fillmore, D., Freitag, S., Ghan, S. J., Ginoux, P., Gong, S., Horowitz, L., Iversen, T., Kirkevåg, A., Klimont, Z., Kondo, Y., Krol, M., Liu, X., Miller, R., Montanaro, V., Moteki, N., Myhre, G., Penner, J. E., Perlitz, J., Pitari, G., Reddy, S., Sahu, L., Sakamoto, H., Schuster, G., Schwarz, J. P., Seland, Ø., Stier, P., Takegawa, N., Takemura, T., Textor, C., van Aardenne, J. A., and Zhao, Y.: Evaluation of black carbon estimations in global aerosol models, *Atmos. Chem. Phys.*, 9, 9001–9026, doi:10.5194/acp-9-9001-2009, 2009.

20 Koffi, B., Schulz, M., Bréon, F.-M., Griesfeller, J., Winker, D., Balkanski, Y., Bauer, S., Berntsen, T., Chin, M., Collins, W. D., Dentener, F., Diehl, T., Easter, R. C., Ghan, S. J., Ginoux, P., Gong, S., Horowitz, L. W., Iversen, T., Kirkevåg, A., Koch, D., Krol, M., Myhre, G., Stier, P., and Takemura, T.: Application of the CALIOP layer product to evaluate the vertical distribution of aerosols estimated by global models: AeroCom phase I results, *J. Geophys. Res.*, 117, D10201, doi:10.1029/2011JD016858, 2012.

25 Korhonen, H., Carslaw, K. S., Spracklen, D. V., Ridley, D. A., and Strom, J.: A global model study of processes controlling aerosol size distributions in the Arctic spring and summer, *J. Geophys. Res.*, 113, D08211, doi:10.1029/2007JD009114, 2008a.

AEROCOM
microphysics
intercomparison

G. W. Mann et al.

[Title Page](#)

[Abstract](#)

[Introduction](#)

[Conclusions](#)

[References](#)

[Tables](#)

[Figures](#)

◀

▶

◀

▶

[Back](#)

[Close](#)

[Full Screen / Esc](#)

[Printer-friendly Version](#)

[Interactive Discussion](#)



- Korhonen, H., Carslaw, K. S., Spracklen, D. V., Mann, G. W., and Woodhouse, M. T.: Influence of ocean dimethyl sulfide emissions on cloud condensation nuclei concentrations and seasonality over the remote Southern Hemisphere oceans: a global model study, *J. Geophys. Res.*, 113, D15204, doi:10.1029/2007JD009718, 2008b.
- 5 Kulmala, M., Laaksonen, A., and Pirjola, L.: Parameterizations for sulfuric acid/water nucleation rates, *J. Geophys. Res.*, 103, 8301–8307, 1998.
- Kulmala, M., Vehkamaki, H., Petajda, T., Dal Maso, M., Lauria, A., Kerminen, V.-M., Birmili, W. and McMurry, P. H.: Formation and growth rates of ultrafine atmospheric particles: a review of observations, *J. Aerosol Sci.*, 35, 143–176, 2004.
- 10 Lamarque, J.-F., Bond, T. C., Eyring, V., Granier, C., Heil, A., Klimont, Z., Lee, D., Liousse, C., Mieville, A., Owen, B., Schultz, M. G., Shindell, D., Smith, S. J., Stehfest, E., Van Aardenne, J., Cooper, O. R., Kainuma, M., Mahowald, N., McConnell, J. R., Naik, V., Riahi, K., and van Vuuren, D. P.: Historical (1850–2000) gridded anthropogenic and biomass burning emissions of reactive gases and aerosols: methodology and application, *Atmos. Chem. Phys.*, 10, 7017–7039, doi:10.5194/acp-10-7017-2010, 2010.
- 15 Lauer, A., Hendricks, J., Ackermann, I., Schell, B., Hass, H., and Metzger, S.: Simulating aerosol microphysics with the ECHAM/MADE GCM – Part I: Model description and comparison with observations, *Atmos. Chem. Phys.*, 5, 3251–3276, doi:10.5194/acp-5-3251-2005, 2005.
- Leaitch, W. R., Banic, C. M., Isaac, G. A., Couture, M. D., Liu, P. S. K., Gultepe, I., Li, S.-M., Kleinman, L., Daum, P. H., and MacPherson, J. I.: Physical and chemical observations in marine stratus during the 1993 North Atlantic Regional Experiment, factors controlling cloud droplet number concentrations, *J. Geophys. Res.*, 101, 29123–29135, 1996.
- 20 Leck, C. and Bigg, E. K.: Biogenic particles in the surface microlayer and overlaying atmosphere in the central Arctic Ocean during summer, *Tellus B*, 57, 305–316, 2005.
- Lee, L. A., Carslaw, K. S., Pringle, K. J., Mann, G. W., and Spracklen, D. V.: Emulation of a complex global aerosol model to quantify sensitivity to uncertain parameters, *Atmos. Chem. Phys.*, 11, 12253–12273, doi:10.5194/acp-11-12253-2011, 2011.
- 25 Lee, L. A., Pringle, K. J., Reddington, C. L., Mann, G. W., Stier, P., Spracklen, D. V., Pierce, J. R., and Carslaw, K. S.: The magnitude and causes of uncertainty in global model simulations of cloud condensation nuclei, *Atmos. Chem. Phys.*, 13, 8879–8914, doi:10.5194/acp-13-8879-2013, 2013.

Title Page	
Abstract	Introduction
Conclusions	References
Tables	Figures
◀	▶
◀	▶
Back	Close
Full Screen / Esc	
Printer-friendly Version	
Interactive Discussion	



Title Page	
Abstract	Introduction
Conclusions	References
Tables	Figures
◀	▶
◀	▶
Back	Close
Full Screen / Esc	
Printer-friendly Version	
Interactive Discussion	

- Lee, Y. H. and Adams, P. J.: Evaluation of aerosol distributions in the GISS-TOMAS global aerosol microphysics model with remote sensing observations, *Atmos. Chem. Phys.*, 10, 2129–2144, doi:10.5194/acp-10-2129-2010, 2010.
- 5 Lee, Y. H., Lamarque, J.-F., Flanner, M. G., Jiao, C., Shindell, D. T., Berntsen, T., Bisiaux, M. M., Cao, J., Collins, W. J., Curran, M., Edwards, R., Faluvegi, G., Ghan, S. J., Horowitz, L. W., McConnell, J. R., Ming, J., Myhre, G., Nagashima, T., Naik, V., Rumbold, S. T., Skeie, R. B., Sudo, K., Takemura, T., Thevenon, F., Xu, B., and Yoon, J.-H.: Evaluation of preindustrial to present-day black carbon and its albedo forcing from Atmospheric Chemistry and Climate Model Intercomparison Project (ACCMIP), *Atmos. Chem. Phys.*, 13, 2607–2634, doi:10.5194/acp-13-2607-2013, 2013.
- Lelieveld, J. and Heintzenberg, J.: Sulfate cooling effect on climate through in-cloud oxidation of anthropogenic SO₂, *Science*, 258, 117–120, 1992.
- 10 Liu, J., Fan, S., Horowitz, L. W., and Levy II, H.: Evaluation of factors controlling long-range transport of black carbon to the Arctic, *J. Geophys. Res.*, 116, D00A14, doi:10.1029/2010JD015145, 2011.
- Liu, X., Penner, J. E., and Herzog, M.: Global modeling of aerosol dynamics: model description, evaluation, and interactions between sulfate and nonsulfate aerosols, *J. Geophys. Res.*, 110, D18206, doi:10.1029/2004JD005674, 2005.
- 15 Liu, X., Easter, R. C., Ghan, S. J., Zaveri, R., Rasch, P., Shi, X., Lamarque, J.-F., Gettelman, A., Morrison, H., Vitt, F., Conley, A., Park, S., Neale, R., Hannay, C., Ekman, A. M. L., Hess, P., Mahowald, N., Collins, W., Iacono, M. J., Bretherton, C. S., Flanner, M. G., and Mitchell, D.: Toward a minimal representation of aerosols in climate models: description and evaluation in the Community Atmosphere Model CAM5, *Geosci. Model Dev.*, 5, 709–739, doi:10.5194/gmd-5-709-2012, 2012.
- 20 Lohmann, U. and Feichter, J.: Global indirect aerosol effects: a review, *Atmos. Chem. Phys.*, 5, 715–737, doi:10.5194/acp-5-715-2005, 2005.
- Luo, G. and Yu, F.: Sensitivity of global cloud condensation nuclei concentrations to primary sulfate emission parameterizations, *Atmos. Chem. Phys.*, 11, 1949–1959, doi:10.5194/acp-11-1949-2011, 2011.
- 25 Lurmann, F. W., Wexler, A. S., Pandis, S. N., Musarra, S., Kumar, N., and Seinfeld, J. H.: Modelling urban and regional aerosols –II. Application to California's south coast air basin, *Atmos. Environ.*, 31, 2695–2715, 1997.



- Mann, G. W., Carslaw, K. S., Spracklen, D. V., Ridley, D. A., Manktelow, P. T., Chipperfield, M. P., Pickering, S. J., and Johnson, C. E.: Description and evaluation of GLOMAP-mode: a modal global aerosol microphysics model for the UKCA composition-climate model, *Geosci. Model Dev.*, 3, 519–551, doi:10.5194/gmd-3-519-2010, 2010.
- Mann, G. W., Carslaw, K. S., Ridley, D. A., Spracklen, D. V., Pringle, K. J., Merikanto, J., Korhonen, H., Schwarz, J. P., Lee, L. A., Manktelow, P. T., Woodhouse, M. T., Schmidt, A., Breider, T. J., Emmerson, K. M., Reddington, C. L., Chipperfield, M. P., and Pickering, S. J.: Intercomparison of modal and sectional aerosol microphysics representations within the same 3-D global chemical transport model, *Atmos. Chem. Phys.*, 12, 4449–4476, doi:10.5194/acp-12-4449-2012, 2012.
- Mann, G. W., Johnson, C. E., Bellouin, N., Dalvi, M., Abraham, L., Carslaw, K. S., Boucher, O., Stier, P., Rae, J., Spracklen, D. V., Telford, P., Pyle, J. A., O'Connor, F., Carver, G., Pringle, K. J., and Woodhouse, M. T.: Evaluation of the new UKCA climate-composition model, Part 3: Tropospheric aerosol properties, in preparation, 2013.
- Martin, G., Johnson, D., and Spice, A.: The measurement and parameterization of effective radius of droplets in warm stratiform clouds, *J. Atmos. Sci.*, 51, 1823–1842, 1994.
- Martensson, E. M., Nilsson, E. D., de Leeuw, G., Cohen, L. H., and Hansson, H.-C.: Laboratory simulations and parameterization of the primary marine aerosol production, *J. Geophys. Res.*, 108, 4297, doi:10.1029/2002JD002263, 2003.
- Merikanto, J., Napari, I., Vehkamaki, H., Anttila, T., and Kulmala, M.: New parameterization of sulfuric acid-ammonia-water ternary nucleation rates at tropospheric conditions, *J. Geophys. Res.*, 112, D15207, doi:10.1029/2006JD007977, 2007.
- Merikanto, J., Spracklen, D. V., Mann, G. W., Pickering, S. J., and Carslaw, K. S.: Impact of nucleation on global CCN, *Atmos. Chem. Phys.*, 9, 8601–8616, doi:10.5194/acp-9-8601-2009, 2009.
- Metzger, A., Verheggen, B., Dommen, J., Duplissy, D., Prevot, A. S. H., Weingartner, E., Riipinen, I., Kulmala, M., Spracklen, D. V., Carslaw, K. S., and Baltensperger, U.: Evidence for the role of organics in aerosol particle formation under atmospheric conditions, *P. Natl. Acad. Sci. USA*, 107, 6646–6651, doi:10.1073/pnas.0911330107, 2010.
- Metzger, S., Dentener, F. Krol, M., Jeuken, A., and Lelieveld, J.: Gas/aerosol partitioning: 2. Global modeling results, *J. Geophys. Res.*, 107, 4313, doi:10.1029/2001JD001103, 2002.
- Myhre, G., Samset, B. H., Schulz, M., Balkanski, Y., Bauer, S., Berntsen, T. K., Bian, H., Bellouin, N., Chin, M., Diehl, T., Easter, R. C., Feichter, J., Ghan, S. J., Hauglustaine, D.,

AEROCOM
microphysics
intercomparison

G. W. Mann et al.

Title Page

Abstract

Introduction

Conclusions

References

Tables

Figures

◀

▶

◀

▶

Back

Close

Full Screen / Esc

Printer-friendly Version

Interactive Discussion



- Iversen, T., Kinne, S., Kirkevåg, A., Lamarque, J.-F., Lin, G., Liu, X., Lund, M. T., Luo, G., Ma, X., van Noije, T., Penner, J. E., Rasch, P. J., Ruiz, A., Selander, Ø., Skeie, R. B., Stier, P., Takemura, T., Tsigaridis, K., Wang, P., Wang, Z., Xu, L., Yu, H., Yu, F., Yoon, J.-H., Zhang, K., Zhang, H., and Zhou, C.: Radiative forcing of the direct aerosol effect from AeroCom Phase II simulations, *Atmos. Chem. Phys.*, 13, 1853–1877, doi:10.5194/acp-13-1853-2013, 2013.
- Napari, I., Noppel, M., Vehkamaki, H., and Kulmala, M.: Parameterization of ternary nucleation rates for $\text{H}_2\text{SO}_4\text{-NH}_3\text{-H}_2\text{O}$ vapours, *J. Geophys. Res.*, 107, 4381, doi:10.1029/2002JD002132, 2002.
- Nenes, A. and Seinfeld, J. H.: Parameterizations of cloud droplet formation in global climate models, *J. Geophys. Res.*, 108, 4415, doi:10.1029/2002JD002911, 2003.
- O'Dowd, C. D. and Smith, M. H.: Physicochemical properties of aerosols over the Northeast Atlantic: evidence for wind-speed-related submicron sea-salt aerosol production, *J. Geophys. Res.*, 98, 1137–1149, 1993.
- O'Dowd, C. D., Geever, M., Hill, M. K., Smith, M. H. and Jennings, S. G.: New particle formation: spatial scales and nucleation rates in the coastal environment, *Geophys. Res. Lett.*, 25, 1661–1664, 1998.
- O'Dowd, C. D., Yoon, Y. J., Junkerman, W., Aalto, P., Kulmala, M., Lihavainen, H., and Viisanen, Y.: Airborne measurements of nucleation mode particles I: coastal nucleation and growth rates, *Atmos. Chem. Phys.*, 7, 1491–1501, doi:10.5194/acp-7-1491-2007, 2007.
- Olivier, J. G. J. and Berdowski, J. J. M.: Global emissions sources and sinks, in: *The Climate System*, edited by: Berdowski, J., Guicherit, R., and Heij, B. J., A. A. Balkema Publishers, Swets and Zeitlinger Publishers, Lisse, the Netherlands, 33–78, 2001.
- Paasonen, P., Asmi, A., Petaja, T., Kajos, M. K., Aijala, M., Junninen, H., Holst, T., Abbatt, J. P. D., Arneth, A., Birmili, W., van der Gon, H. D., Hamed, A., Hoffer, A., Laakso, L., Laaksonen, A., Leaitch, W. R., Plass-Dulmer, C., Pryor, S. C., Raisanen, P., Swietlicki, E., Wiedensohler, A., Worsnop, D. R., Kerminen, V.-M., and Kulmala, M.: Warming-induced increase in aerosol number concentration likely to moderate climate change, *Nat. Geosci.*, 6, 438–442, 2013.
- Penner, J. E., Quaas, J., Storelvmo, T., Takemura, T., Boucher, O., Guo, H., Kirkevåg, A., Kristjánsson, J. E., and Selander, Ø.: Model intercomparison of indirect aerosol effects, *Atmos. Chem. Phys.*, 6, 3391–3405, doi:10.5194/acp-6-3391-2006, 2006.
- Petzold, A., Fiebig, M., Flentje, H., Keil, A., Leiterer, U., Schroeder, F., Stifter, A., Wendisch, M., and Wendling, P.: Vertical variability of aerosol properties observed at a continental site dur-

Title Page	
Abstract	Introduction
Conclusions	References
Tables	Figures
	
	
Back	Close
Full Screen / Esc	
Printer-friendly Version	
Interactive Discussion	



**AEROCOM
microphysics
intercomparison**

G. W. Mann et al.

[Title Page](#)[Abstract](#)[Introduction](#)[Conclusions](#)[References](#)[Tables](#)[Figures](#)[◀](#)[▶](#)[Back](#)[Close](#)[Full Screen / Esc](#)[Printer-friendly Version](#)[Interactive Discussion](#)

AEROCOM
microphysics
intercomparison

G. W. Mann et al.

Title Page

Abstract

Introduction

Conclusions

References

Tables

Figures

◀

▶

◀

▶

Back Close

Full Screen / Esc

Printer-friendly Version

Interactive Discussion



**AEROCOM
microphysics
intercomparison**

G. W. Mann et al.

[Title Page](#)[Abstract](#)[Introduction](#)[Conclusions](#)[References](#)[Tables](#)[Figures](#)[|◀](#)[▶|](#)[◀](#)[▶|](#)[Back](#)[Close](#)[Full Screen / Esc](#)[Printer-friendly Version](#)[Interactive Discussion](#)

the European boundary layer, *Atmos. Chem. Phys.*, 11, 12007–12036, doi:10.5194/acp-11-12007-2011, 2011.

Remer, L. A., Kleidman, R. G., Levy, R. C., Kaufman, Y. J., Tanre, D. T., Mattoo, S., Vanderlei-Martins, J., Ichoku, C., Koren, I., Yu, H., and Holben, B. N.: Global aerosol climatology from the MODIS satellite sensors, *J. Geophys. Res.*, 113, D14S07, doi:10.1029/2007JD009661, 2008.

Samset, B. H., Myhre, G., Schulz, M., Balkanski, Y., Bauer, S., Berntsen, T. K., Bian, H., Beliouin, N., Diehl, T., Easter, R. C., Ghan, S. J., Iversen, T., Kinne, S., Kirkevåg, A., Lamarque, J.-F., Lin, G., Liu, X., Penner, J. E., Seland, Ø., Skeie, R. B., Stier, P., Takemura, T., Tsigaridis, K., and Zhang, K.: Black carbon vertical profiles strongly affect its radiative forcing uncertainty, *Atmos. Chem. Phys.*, 13, 2423–2434, doi:10.5194/acp-13-2423-2013, 2013.

Schmidt, A., Carslaw, K. S., Mann, G. W., Rap, A., Pringle, K. J., Spracklen, D. V., Wilson, M., and Forster, P. M.: Importance of tropospheric volcanic aerosol for indirect radiative forcing of climate, *Atmos. Chem. Phys.*, 12, 7321–7339, doi:10.5194/acp-12-7321-2012, 2012.

Schulz, M., Textor, C., Kinne, S., Balkanski, Y., Bauer, S., Berntsen, T., Berglen, T., Boucher, O., Dentener, F., Guibert, S., Isaksen, I. S. A., Iversen, T., Koch, D., Kirkevåg, A., Liu, X., Montanaro, V., Myhre, G., Penner, J. E., Pitari, G., Reddy, S., Seland, Ø., Stier, P., and Takemura, T.: Radiative forcing by aerosols as derived from the AeroCom present-day and pre-industrial simulations, *Atmos. Chem. Phys.*, 6, 5225–5246, doi:10.5194/acp-6-5225-2006, 2006.

Schulz, M., Chin, M., and Kinne, S.: The Aerosol Model Comparison Project, AeroCom, Phase II: Clearing Up Diversity, International Global Atmospheric Chemistry Newsletter, No. 41, (<http://www.igacproject.org/Newsletters>), 2009.

Schwarz, J. P., Spackman, J. R., Gao, R. S., Watts, L. A., Stier, P., Schulz, M., Davis, S. M., Wofsy, S. C., and Fahey, D. W.: Global-scale black carbon profiles observed in the remote atmosphere and compared to models, *Geophys. Res. Lett.*, 37, L18812, doi:10.1029/2010GL044372, 2010.

Scott, C. E., Rap, A., Spracklen, D. V., Forster, P. M., Carslaw, K. S., Mann, G. W., Pringle, K. J., Kivekäs, N., Kulmala, M., Lihavainen, H., and Tunved, P.: The direct and indirect radiative effects of biogenic secondary organic aerosol, *Atmos. Chem. Phys. Discuss.*, 13, 16961–17019, doi:10.5194/acpd-13-16961-2013, 2013.

Sihto, S.-L., Kulmala, M., Kerminen, V.-M., Dal Maso, M., Petäjä, T., Riipinen, I., Korhonen, H., Arnold, F., Janson, R., Boy, M., Laaksonen, A., and Lehtinen, K. E. J.: Atmospheric sulphuric acid and aerosol formation: implications from atmospheric measurements for nucle-

- ation and early growth mechanisms, *Atmos. Chem. Phys.*, 6, 4079–4091, doi:10.5194/acp-6-4079-2006, 2006.

Spracklen, D. V., Pringle, K. J., Carslaw, K. S., Chipperfield, M. P., and Mann, G. W.: A global off-line model of size-resolved aerosol microphysics: I. Model development and prediction of aerosol properties, *Atmos. Chem. Phys.*, 5, 2227–2252, doi:10.5194/acp-5-2227-2005, 2005.

Spracklen, D. V., Pringle, K. J., Carslaw, K. S., Chipperfield, M. P., and Mann, G. W.: A global off-line model of size-resolved aerosol microphysics: II. Identification of key uncertainties, *Atmos. Chem. Phys.*, 5, 3233–3250, doi:10.5194/acp-5-3233-2005, 2005.

Spracklen, D. V., Carslaw, K. S., Kulmala, M., Kerminen, V.-M., Mann, G. W., and Sihto, S.-L.: The contribution of boundary layer nucleation events to total particle concentrations on regional and global scales, *Atmos. Chem. Phys.*, 6, 5631–5648, doi:10.5194/acp-6-5631-2006, 2006.

Spracklen, D. V., Pringle, K. J., Carslaw, K. S., Mann, G. W., Manktelow, P., and Heintzenberg, J.: Evaluation of a global aerosol microphysics model against size-resolved particle statistics in the marine atmosphere, *Atmos. Chem. Phys.*, 7, 2073–2090, doi:10.5194/acp-7-2073-2007, 2007.

Spracklen, D. V., Carslaw, K. S., Kulmala, M., Kerminen, V.-M., Sihto, S.-L., Riipinen, I., Merikanto, J., Mann, G. W., Chipperfield, M. P., Wiedensohler, A., Birmili, W. and Lihavainen, H.: Contribution of particle formation to global cloud condensation nuclei concentrations, *Geophys. Res. Lett.*, 35, L06808, doi:10.1029/2007GL033038, 2008.

Spracklen, D. V., Carslaw, K. S., Merikanto, J., Mann, G. W., Reddington, C. L., Pickering, S., Ogren, J. A., Andrews, E., Baltensperger, U., Weingartner, E., Boy, M., Kulmala, M., Laakso, L., Lihavainen, H., Kivekäs, N., Komppula, M., Mihalopoulos, N., Kouvarakis, G., Jennings, S. G., O'Dowd, C., Birmili, W., Wiedensohler, A., Weller, R., Gras, J., Laj, P., Sellegrí, K., Bonn, B., Krejci, R., Laaksonen, A., Hamed, A., Minikin, A., Harrison, R. M., Talbot, R., and Sun, J.: Explaining global surface aerosol number concentrations in terms of primary emissions and particle formation, *Atmos. Chem. Phys.*, 10, 4775–4793, doi:10.5194/acp-10-4775-2010, 2010.

Spracklen, D. V., Carslaw, K. S., Pöschl, U., Rap, A., and Forster, P. M.: Global cloud condensation nuclei influenced by carbonaceous combustion aerosol, *Atmos. Chem. Phys.*, 11, 9067–9087, doi:10.5194/acp-11-9067-2011, 2011.

- Stier, P., Feichter, J., Kinne, S., Kloster, S., Vignati, E., Wilson, J., Ganzeveld, L., Tegen, I., Werner, M., Balkanski, Y., Schulz, M., Boucher, O., Minikin, A., and Petzold, A.: The aerosol-climate model ECHAM5-HAM, *Atmos. Chem. Phys.*, 5, 1125–1156, doi:10.5194/acp-5-1125-2005, 2005.
- 5 Stier, P., Schutgens, N. A. J., Bellouin, N., Bian, H., Boucher, O., Chin, M., Ghan, S. J., Huneeus, N., Kinne, S., Lin, G., Ma, X., Myhre, G., Penner, J. E., Randles, C. A., Samset, B., Schulz, M., Takemura, T., Yu, F., Yu, H., and Zhou, C.: Host model uncertainties in aerosol radiative forcing estimates: results from the AeroCom Prescribed intercomparison study, *Atmos. Chem. Phys.*, 13, 3245–3270, doi:10.5194/acp-13-3245-2013, 2013.
- 10 Tanre, D., Kaufman, Y. J., Herman, M., and Mattoo, S.: Remote sensing of aerosol properties over ocean using the MODIS/EOS spectral radiances, *J. Geophys. Res.*, 102, 16971–16988, 1997.
- Telford, P. J., Braesicke, P., Morgenstern, O., and Pyle, J. A.: Technical Note: Description and assessment of a nudged version of the new dynamics Unified Model, *Atmos. Chem. Phys.*, 8, 1701–1712, doi:10.5194/acp-8-1701-2008, 2008.
- 15 Textor, C., Schulz, M., Guibert, S., Kinne, S., Balkanski, Y., Bauer, S., Berntsen, T., Berglen, T., Boucher, O., Chin, M., Dentener, F., Diehl, T., Easter, R. C., Feichter, H., Fillmore, D., Ghan, S. J., Ginoux, P., Gong, S., Grini, A., Hendricks, J., Horowitz, L., Huang, P., Isaksen, I., Iversen, I., Kloster, S., Koch, D., Kirkevåg, A., Kristjansson, J. E., Krol, M., Lauer, A., Lamarque, J. F., Liu, X., Montanaro, V., Myhre, G., Penner, J., Pitari, G., Reddy, S., Seland, Ø., Stier, P., Takemura, T., and Tie, X.: Analysis and quantification of the diversities of aerosol life cycles within AeroCom, *Atmos. Chem. Phys.*, 6, 1777–1813, doi:10.5194/acp-6-1777-2006, 2006.
- 20 Textor, C., Schulz, M., Guibert, S., Kinne, S., Balkanski, Y., Bauer, S., Berntsen, T., Berglen, T., Boucher, O., Chin, M., Dentener, F., Diehl, T., Feichter, J., Fillmore, D., Ginoux, P., Gong, S., Grini, A., Hendricks, J., Horowitz, L., Huang, P., Isaksen, I. S. A., Iversen, T., Kloster, S., Koch, D., Kirkevåg, A., Kristjansson, J. E., Krol, M., Lauer, A., Lamarque, J. F., Liu, X., Montanaro, V., Myhre, G., Penner, J. E., Pitari, G., Reddy, M. S., Seland, Ø., Stier, P., Takemura, T., and Tie, X.: The effect of harmonized emissions on aerosol properties in global models – an AeroCom experiment, *Atmos. Chem. Phys.*, 7, 4489–4501, doi:10.5194/acp-7-4489-2007, 2007.
- 25
- 30

Title Page	
Abstract	Introduction
Conclusions	References
Tables	Figures
◀	▶
◀	▶
Back	Close
Full Screen / Esc	
Printer-friendly Version	
Interactive Discussion	



Thomson, A. M., Calvin, K. V., Smith, S. J., Page Kyle, G., Volke, A., Patel, P., Delgado-Arias, S., Bond-Lamberty, B., Wise, M. A., Clarke, L. E., and Edmonds, J. A.: RCP4.5: a pathway for stabilisation of radiative forcing by 2100, *Clim. Change*, 109, 77–94, 2011.

Torres, O., Barthia, P. K., Herman, J. R., Sinyuk, A., Ginoux, P., and Holben, B.: A long-term record of aerosol optical depth from TOMS observations and comparisons to AERONET measurements, *J. Atmos. Sci.*, 59, 398–413, 2002.

Trivitayanurak, W., Adams, P. J., Spracklen, D. V., and Carslaw, K. S.: Tropospheric aerosol microphysics simulation with assimilated meteorology: model description and intermodel comparison, *Atmos. Chem. Phys.*, 8, 3149–3168, doi:10.5194/acp-8-3149-2008, 2008.

Tsigaridis, K., Daskalakis, N., Kanakidou, M., Adams, P. J., Artaxo, P., Bahadur, R., Balkanski, Y., Bauer, S. E., Bellouin, N., Benedetti, A., Bergman, T., Berntsen, T. K., Beukes, J. P., Bian, H., Carslaw, K. S., Chin, M., Curci, G., Diehl, T., Easter, R. C., Ghan, S. J., Gong, S. L., Hodzic, A., Hoyle, C. R., Iversen, T., Jathar, S., Jimenez, J.-L., Kaiser, J. W., Kirkevag, A., Koch, D., Kokkola, H., Lee, Y. H., Lin, G., Liu, X., Luo, G., Ma, X., Mann, G. W., Mihalopoulos, N., Morcrette, J.-J., Muller, J.-F., Myhre, G., Myrookefalitakis, S., Ng, S., O'Donnell, D., Penner, J. E., Pozzoli, L., Pringle, K. J., Russell, L. M., Schulz, M., Sciare, J., Selander, O., Shindell, D. T., Sillman, S., Skeie, R. B., Spracklen, D. V., Stavrakou, J., Steenrod, S. D., Strunk, A., Takemura, T., Tiiitta, P., Tilmes, S., Tost, H., van Noije, T., von Salzen, K., Yu, F., Wang, Z., Wang, Z., Zaveri, R., Zhang, H., Zhang, K., Zhang, Q., and Zhang, X.: An AeroCom intercomparison exercise on state-of-the-art organic aerosol global modeling, in preparation, 2013.

Van Dingenen, R., Raes, F., and Jenson, N. R.: Evidence for anthropogenic impact on number concentration and sulfate content of cloud-processed aerosol particles over the North Atlantic, *J. Geophys. Res.*, 100, 21057–21067, 1995.

Van Dingenen, R., Raes, F., Putaud, J.-P., Baltensperger, U., Charron, A., Facchini, M. C., Decesari, S., Fuzzi, S., Gehrig, R., Hansson, H. C., Harrison, R. M., Huglin, C., Jones, A. M., Laj, P., Lorbeer, G., Maenhaut, W., Palmgren, F., Querol, X., Rodriguez, S., Schneider, J., Ten Brink, H., Tunved, P., a Torseth, K., Wehner, B., Weingartner, E., Wiedensohler, A. and Waehlin, P.: A European aerosol phenomenology – 1: physical characteristics of particulate matter at kerbside, urban, rural and background sites in Europe, *Atmos. Environ.* 38, 2561–2577, 2004.

Vehkamaki, H., Kulmala, M., Napari, I., Lehtinen, K. E. J., Timmreck, C., Noppel, M., and Laaksonen, A.: An improved parameterization for sulfuric acid-water nucleation

Title Page

Abstract

Introduction

Conclusions

References

Tables

Figures

◀

▶

◀

▶

Back

Close

Full Screen / Esc

Printer-friendly Version

Interactive Discussion



- rates for tropospheric and stratospheric conditions, *J. Geophys. Res.*, 107, 4622, doi:10.1029/2002JD002184, 2002.
- Vignati, E., Wilson, J., and Stier, P.: M7: an efficient size-resolved aerosol microphysics module for large-scale aerosol transport models, *J. Geophys. Res.*, 109, D22202, doi:10.1029/2003JD004485, 2004.
- Vignati, E., Karl, M., Krol, M., Wilson, J., Stier, P., and Cavalli, F.: Sources of uncertainties in modelling black carbon at the global scale, *Atmos. Chem. Phys.*, 10, 2595–2611, doi:10.5194/acp-10-2595-2010, 2010.
- von Salzen, K.: Piecewise log-normal approximation of size distributions for aerosol modelling, *Atmos. Chem. Phys.*, 6, 1351–1372, doi:10.5194/acp-6-1351-2006, 2006.
- Whitby, E. and McMurry, P.: Modal aerosol dynamics modeling, *Aerosol. Sci. Tech.*, 27, 673–688, 1997.
- Whitby, K. T.: The physical characteristics of sulfur aerosols, *Atmos. Environ.*, 12, 135–159, 1978.
- Wiedensohler, A., Birmili, W., Nowak, A., Sonntag, A., Weinhold, K., Merkel, M., Wehner, B., Tuch, T., Pfeifer, S., Fiebig, M., Fjäraa, A. M., Asmi, E., Sellegri, K., Depuy, R., Venzac, H., Villani, P., Laj, P., Aalto, P., Ogren, J. A., Swietlicki, E., Williams, P., Roldin, P., Quincey, P., Hüglin, C., Fierz-Schmidhauser, R., Gysel, M., Weingartner, E., Riccobono, F., Santos, S., Grüning, C., Faloon, K., Beddows, D., Harrison, R., Monahan, C., Jennings, S. G., O'Dowd, C. D., Marinoni, A., Horn, H.-G., Keck, L., Jiang, J., Scheckman, J., McMurry, P. H., Deng, Z., Zhao, C. S., Moerman, M., Henzing, B., de Leeuw, G., Löschau, G., and Basstian, S.: Mobility particle size spectrometers: harmonization of technical standards and data structure to facilitate high quality long-term observations of atmospheric particle number size distributions, *Atmos. Meas. Tech.*, 5, 657–685, doi:10.5194/amt-5-657-2012, 2012.
- Wilson, J., Cuvelier, C., and Raes, F.: A modeling study of global mixed aerosol fields, *J. Geophys. Res.*, 106, 34081–34108, 2001.
- Yu, F.: From molecular clusters to nanoparticles: second-generation ion-mediated nucleation model, *Atmos. Chem. Phys.*, 6, 5193–5211, doi:10.5194/acp-6-5193-2006, 2006.
- Yu, F.: Ion-mediated nucleation in the atmosphere: key controlling parameters, implications, and look-up table, *J. Geophys. Res.*, 115, D03206, doi:10.1029/2009JD012630, 2010.
- Yu, F. and Luo, G.: Simulation of particle size distribution with a global aerosol model: contribution of nucleation to aerosol and CCN number concentrations, *Atmos. Chem. Phys.*, 9, 7691–7710, doi:10.5194/acp-9-7691-2009, 2009.

[Title Page](#)[Abstract](#)[Introduction](#)[Conclusions](#)[References](#)[Tables](#)[Figures](#)[◀](#)[▶](#)[◀](#)[▶](#)[Back](#)[Close](#)[Full Screen / Esc](#)[Printer-friendly Version](#)[Interactive Discussion](#)

- Yu, F., Luo, G., Bates, T., Anderson, B., Clarke, A., Kapustin, V., Yantosca, R., Wang, Y., and Wu, S.: Spatial distributions of particle number concentrations in the global troposphere: simulations, observations, and implications for nucleation mechanisms, *J. Geophys. Res.*, 115, D17205, doi:10.1029/2009JD013473, 2010.
- 5 Zhang, K., Wan, H., Wang, B., Zhang, M., Feichter, J., and Liu, X.: Tropospheric aerosol size distributions simulated by three online global aerosol models using the M7 microphysics module, *Atmos. Chem. Phys.*, 10, 6409–6434, doi:10.5194/acp-10-6409-2010, 2010.
- Zhang, K., O'Donnell, D., Kazil, J., Stier, P., Kinne, S., Lohmann, U., Ferrachat, S., Croft, B., Quaas, J., Wan, H., Rast, S., and Feichter, J.: The global aerosol-climate model ECHAM-HAM, version 2: sensitivity to improvements in process representations, *Atmos. Chem. Phys.*, 12, 8911–8949, doi:10.5194/acp-12-8911-2012, 2012.
- 10

Title Page	
Abstract	Introduction
Conclusions	References
Tables	Figures
◀	▶
◀	▶
Back	Close
Full Screen / Esc	
Printer-friendly Version	
Interactive Discussion	



AEROCOM microphysics intercomparison

G. W. Mann et al.

Table 1. List of participating global aerosol microphysics models. Two-moment schemes (2m) carry number and mass in each size class whereas single-moment (1m) schemes carry only mass. Most models are modal or sectional but CanAM4-PAM uses the piecewise log-normal approach (pcwise-lgnrml). Schemes running in free-running (free) General Circulation Models (GCMs) submitted multi-annual monthly means from 5 yr simulations whereas nudged (nudg) GCMs and CTMs submitted monthly-mean results driven by 2006 meteorological re-analyses.

Model	Scheme type	Classes	Tracers	Host model	Resolution	Reference
CAM5-MAM3	modal (2m)	3	15	GCM (free)	$1.9^\circ \times 2.5^\circ \times L30$	Liu et al. (2012)
HadGEM3-UKCA	modal (2m)	5	20	GCM (nudg)	$1.3^\circ \times 1.9^\circ \times L63$	Mann et al. (2013)
TM5	modal (2m)	7	25	CTM	$2.0^\circ \times 3.0^\circ \times L34$	Aan de Brugh et al. (2011)
GLOMAP-mode	modal (2m)	7	26	CTM	$2.8^\circ \times 2.8^\circ \times L31$	Mann et al. (2012)
EMAC	modal (2m)	7	41	GCM (nudg)	$2.8^\circ \times 2.8^\circ \times L19$	Pringle et al. (2010)
ECHAM5-HAM2	modal (2m)	7	29 ^a	GCM (nudg)	$1.9^\circ \times 1.9^\circ \times L31$	Zhang et al. (2012)
GISS-MATRIX	modal ^b (2m)	16	60	GCM (nudg)	$2.0^\circ \times 2.5^\circ \times L40$	Bauer et al. (2008)
CanAM4-PAM	pcwise-lgnrml (2m)	7	20	GCM (free)	$3.7^\circ \times 3.7^\circ \times L35$	Von Salzen (2006)
GEOS-Chem-APM	sectional (1m)	100	100	CTM	$2.0^\circ \times 2.5^\circ \times L47$	Yu and Luo (2009)
ECHAM5-SALSA	sectional (2m)	20	65	GCM (nudg)	$1.9^\circ \times 1.9^\circ \times L31$	Bergman et al. (2012)
GISS-TOMAS	sectional (2m)	12	72	GCM (free)	$4.0^\circ \times 5.0^\circ \times L09$	Lee and Adams (2010)
GLOMAP-bin	sectional (2m)	40	160	CTM	$2.8^\circ \times 2.8^\circ \times L31$	Spracklen et al. (2005a, 2011)

^a Although treatment of SOA in ECHAM5-HAM2 involves 20 SOA species, only 4 additional advected aerosol tracers are required in addition to the 25 for ECHAM5-HAM. Another 4 species are required for the condensable organic gases.

^b Note that GISS-MATRIX scheme follows the quadrature method of moments.

Title Page	
Abstract	Introduction
Conclusions	References
Tables	Figures
Back	Close
Full Screen / Esc	
Printer-friendly Version	
Interactive Discussion	



**AEROCOM
microphysics
intercomparison**

G. W. Mann et al.

[Title Page](#)[Abstract](#)[Introduction](#)[Conclusions](#)[References](#)[Tables](#)[Figures](#)[Back](#)[Close](#)[Full Screen / Esc](#)[Printer-friendly Version](#)[Interactive Discussion](#)

Table 2. Treatment of emissions, oxidants and nucleation in each model. Abbreviations for emissions are AERO-00 (Dentener et al., 2006), HCA-06 (Diehl et al., 2012), IPCC-00 (Lamarque et al., 2010), IPCC-06 (RCP4.5 for 2006, Thomson et al., 2011). The primary size assumptions correspond to the geometric mean diameter values (nm) for primary carbonaceous particle emissions. The comma-separated values shown are for fossil fuel and biofuel sources respectively with geometric standard deviation also shown in parentheses. Nucleation parameterizations are abbreviated as BHN (binary homogeneous nucleation), BLN (activation boundary layer nucleation), THN (ternary homogeneous nucleation), IIN (ion-induced nucleation) and IMN (ion-mediated nucleation). References for nucleation parameterizations are V02 (Vehkamaki et al., 2002), S06 (Sihto et al., 2006), M07 (Merikanto et al., 2007), K98 (Kulmala et al., 1998), K10 (Kazil et al., 2010), N02 (Napari et al., 2002) and Y10 (Yu, 2010). Also shown is each model's column global burdens of sulphate (Tg of sulphur) and BC (Tg of carbon), and global mean surface number concentrations (cm^{-3}) of particles with dry diameter larger than 30 nm (N_{30}) and 100 nm (N_{100}).

Model	Emissions	Primary size	Oxidants	Nucleation	SO_4	BC	N_{30}	N_{100}
CAM5-MAM3	IPCC-00	80, 80 (1.80,1.80)	prescribed	BHN (V02) and BLN (S06)	0.42	0.08	447	231
HadGEM3-UKCA	IPCC-00	60, 150 (1.59,1.59)	online	BHN (V02)	0.60	0.10	425	198
TM5	IPCC-06	30, 30 (1.59,1.59)	online	BHN (V02)	0.51	0.16	1535	186
GLOMAP-mode	HCA-06	30, 80 (1.80,1.80)	prescribed	BHN (K98)	0.75	0.11	527	313
EMAC	AERO-00	60, 150 (1.59,1.59)	online	BHN (V02)	0.38	0.20	1140	405
ECHAM5-HAM2	HCA-06	60, 60 (1.59,1.59)	prescribed	IIN (K10)	0.94	0.12	490	199
GISS-MATRIX	IPCC-00	50, 100 (1.80,1.80)	online	THN (N02)	0.60	0.09	213	108
CanAM4-PAM	HCA-06	30, 80 (1.80,1.80)	prescribed	THN (M07)	0.61	0.15	1868	480
GEOS-Chem-APM	AERO-00*	60, 150 (1.80,1.80)	online	IMN (Y10)	0.59	0.12	705	274
ECHAM5-SALSA	HCA-06	60, 150 (1.59,1.59)	prescribed	BHN (V02)	0.61	0.08	380	154
GISS-TOMAS	AERO-00	30, 80 (1.80,1.80)	prescribed	BHN (V02)	1.39	0.11	1129	379
GLOMAP-bin	HCA-06	30, 80 (1.80,1.80)	prescribed	BHN (K98)	0.80	0.12	972	411

* Except for anthropogenic SO_2 and NO_x which is based on the Emissions Database for Global Atmospheric Research (EDGAR) inventory (Olivier and Berdowski, 2001) and scaled to year 2006 with also some improved estimates from other inventories for several regions (G. Luo, personal communication, 2013).

Table 3. Observational datasets on size-resolved number concentrations used in the evaluation of the multi global aerosol microphysics models.

Dataset	Environment	Instrument	Quantity compared	Location	Data duration
GAW-WDCA	Free Trop.	CPC	N_{10}, N_{10}, N_{14}	JFJ, MLO, SPO	11, 24, 25 yr
GAW-WDCA	Marine BL	CPC	$N_{10}, N_{14}, N_{14}, N_{14}, N_3$	MHT, NEU, BRW, SMO, THD, CGR	6, 13, 31, 20, 5, 7 yr
GAW-WDCA	Cont'l BL	CPC	$N_{10}, N_{14}, N_{10}, N_3$	SGP, BND, PAS, HOP	11, 13, 6, 10 yr
EUSAAR	Nordic/Baltic BL	D/SMPS	N_{30}, N_{50}, N_{100} , size dis	ASP, BIR, SMR, PAL, PLA, VHL	2 yr (2008/09)
EUSAAR-GUAN	C. Europe BL	D/SMPS	N_{30}, N_{50}, N_{100} , size dis	BOS, HPB, KPO, OBK, MPZ, WAL	2 yr (2008/09)
EUSAAR	W. Europe BL	D/SMPS	N_{30}, N_{50}, N_{100} , size dis	CBW, HWL, MHT, JRC	2 yr (2008/09)
EUSAAR	Mediterranean BL	D/SMPS	N_{30}, N_{50}, N_{100} , size dis	FKL	2 yr (2008/09)
EUSAAR	Arctic BL	D/SMPS	N_{30}, N_{50}, N_{100} , size dis	ZEP	2 yr (2008/09)
LACE campaign	C. Europe BL/FT	CPC, PCASP	N_5, N_{15}, N_{120}	Over eastern Germany	summer 1998
Heintzenberg	marine BL	DMPS/APS	sub- μm size dis	75° S to 90° N	30 yr
Clarke	marine BL/FT	u-CPC	N_3	Pacific and S. Ocean	10+ yr

[Title Page](#)[Abstract](#)[Introduction](#)[Conclusions](#)[References](#)[Tables](#)[Figures](#)[|◀](#)[▶|](#)[◀](#)[▶](#)[Back](#)[Close](#)[Full Screen / Esc](#)[Printer-friendly Version](#)[Interactive Discussion](#)

**AEROCOM
microphysics
intercomparison**

G. W. Mann et al.

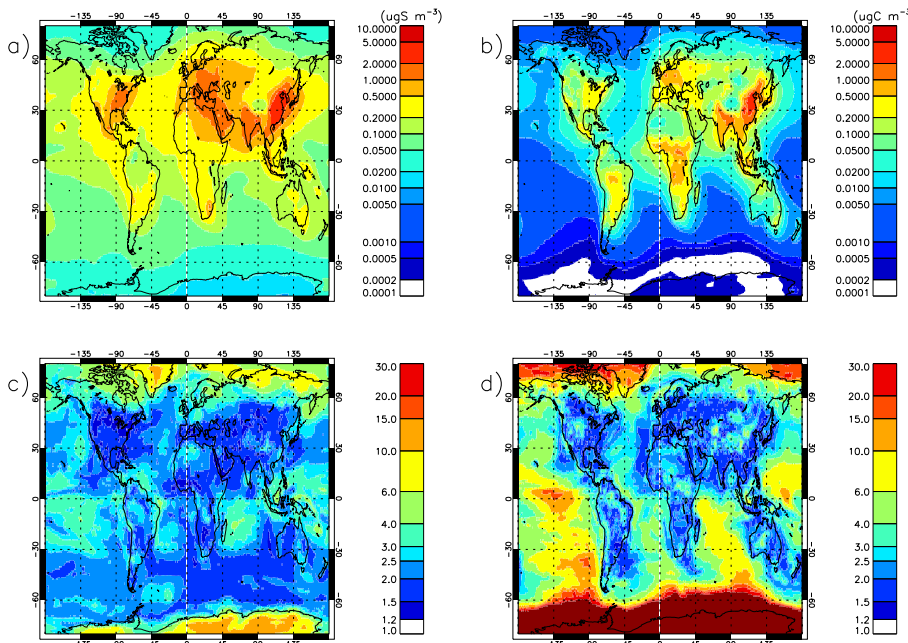


Fig. 1. Global maps of central-8 model mean and diversity for simulated annual mean surface mass concentrations of sulphate (**a, c**) and black carbon (**b, d**). Note that the geometric mean is used when averaging over the central-8 models.

[Title Page](#)[Abstract](#)[Introduction](#)[Conclusions](#)[References](#)[Tables](#)[Figures](#)[|◀](#)[▶|](#)[Back](#)[Close](#)[Full Screen / Esc](#)[Printer-friendly Version](#)[Interactive Discussion](#)

AEROCOM
microphysics
intercomparison

G. W. Mann et al.

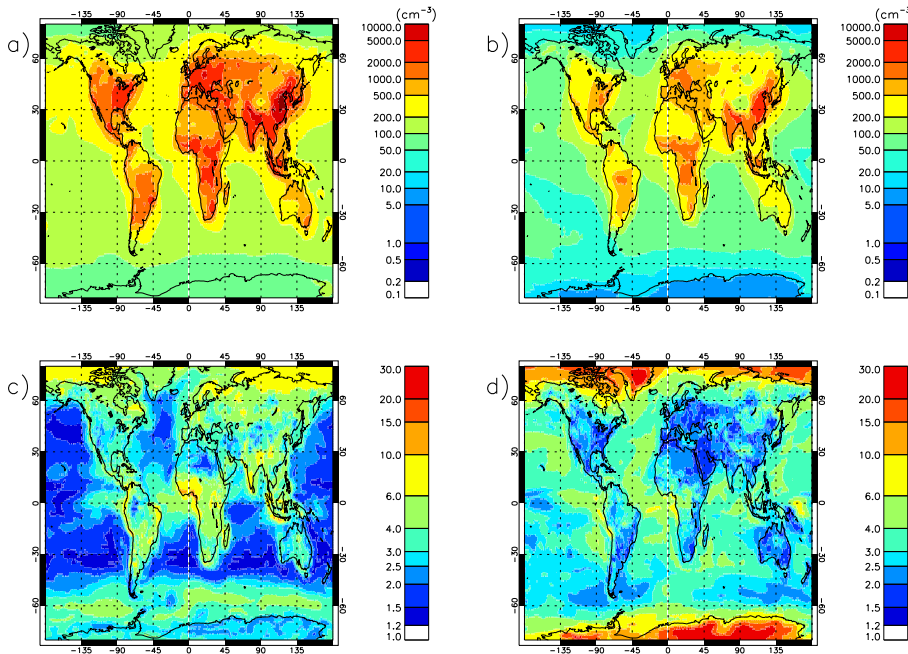


Fig. 2. Global maps of central-8 model mean and diversity for simulated annual mean surface size-resolved number concentrations for $N(D_p > 30 \text{ nm})$ (**a, c**) and $N(D_p > 100 \text{ nm})$ (**b, d**). Note that the geometric mean is used when averaging over the central-8 models.

- [Title Page](#)
- [Abstract](#) [Introduction](#)
- [Conclusions](#) [References](#)
- [Tables](#) [Figures](#)
- [◀](#) [▶](#)
- [◀](#) [▶](#)
- [Back](#) [Close](#)
- [Full Screen / Esc](#)
- [Printer-friendly Version](#)
- [Interactive Discussion](#)

AEROCOM microphysics intercomparison

G. W. Mann et al.

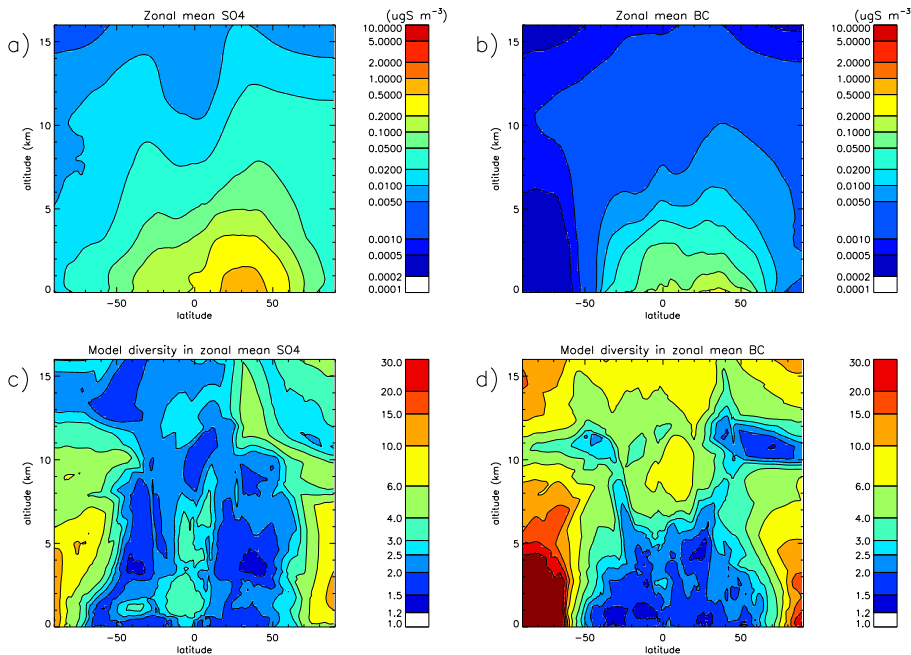


Fig. 3. Zonal-mean vs. latitude and altitude plots of central-8 model mean and diversity for simulated annual mean mass concentrations of sulphate (**a, c**) and black carbon (**b, d**). Note that the geometric mean is used when averaging over the central-8 models.

[Title Page](#)

[Abstract](#)

[Introduction](#)

[Conclusions](#)

[References](#)

[Tables](#)

[Figures](#)

[|◀](#)

[▶|](#)

[Back](#)

[Close](#)

[Full Screen / Esc](#)

[Printer-friendly Version](#)

[Interactive Discussion](#)



AEROCOM microphysics intercomparison

G. W. Mann et al.

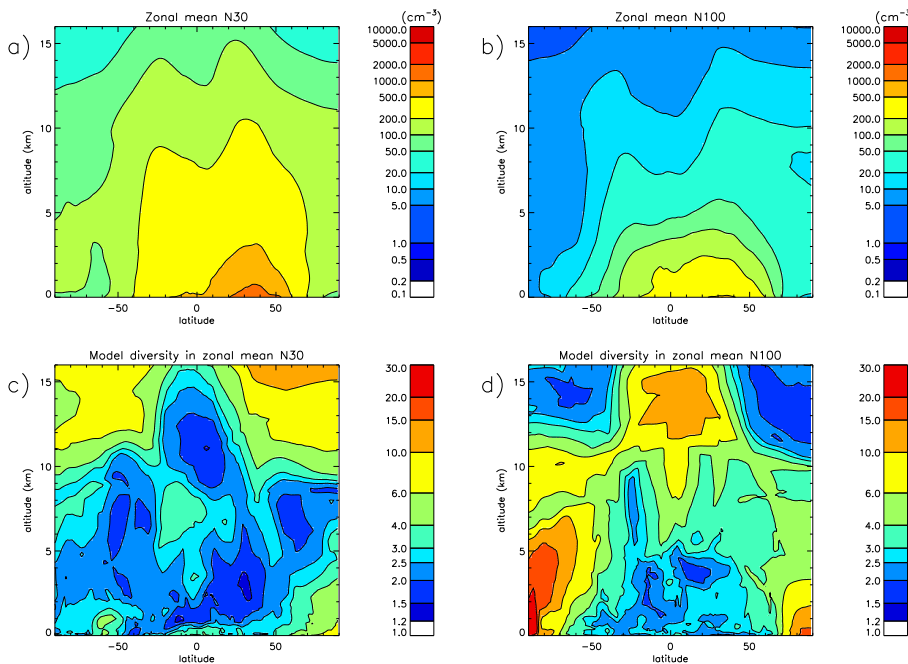


Fig. 4. Zonal-mean vs. latitude and altitude plots of central-8 model mean and diversity for simulated annual mean size-resolved number concentrations for $N(D_p > 30 \text{ nm})$ (**a, c**) and $N(D_p > 100 \text{ nm})$ (**b, d**). Note that the geometric mean is used when averaging over the central-8 models.

- [Title Page](#)
- [Abstract](#) [Introduction](#)
- [Conclusions](#) [References](#)
- [Tables](#) [Figures](#)
- [◀](#) [▶](#)
- [◀](#) [▶](#)
- [Back](#) [Close](#)
- [Full Screen / Esc](#)
- [Printer-friendly Version](#)
- [Interactive Discussion](#)

**AEROCOM
microphysics
intercomparison**

G. W. Mann et al.

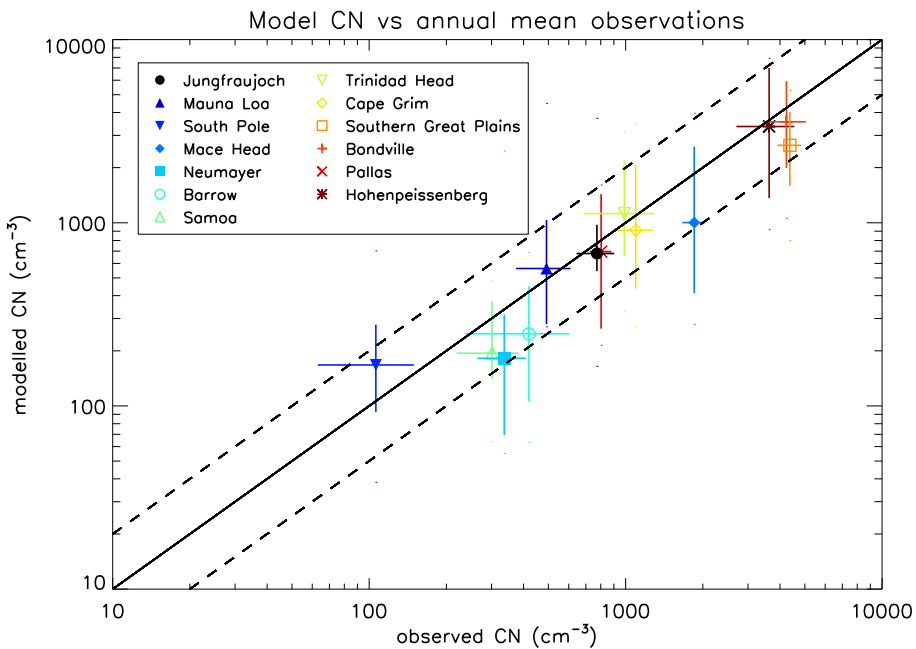


Fig. 5. Simulated annual mean surface $N(D_p > 3/10/14 \text{ nm})$ against CPC observations at all 13 GAW sites. The model values are geometric means over the central 8 models with the vertical whisker indicating their range. For the observations, the multi-annual mean is shown with the horizontal whisker plus and minus the standard deviation over the several years of data shown in Table 3.

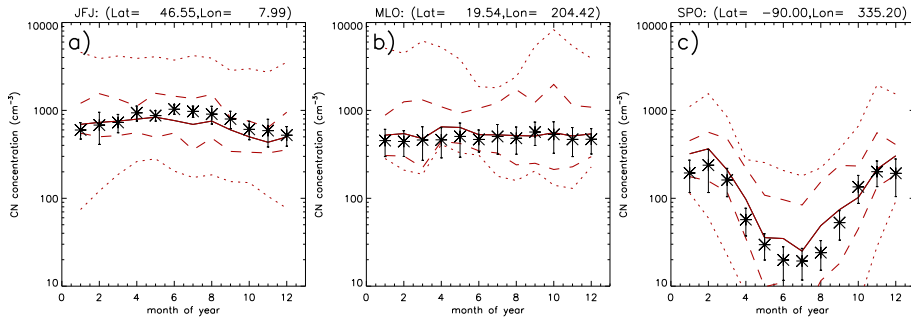


Fig. 6. Simulated annual cycle in surface $N(D_p > 10 \text{ nm}/14 \text{ nm})$ against CPC observations at free troposphere GAW sites (Jungfraujoch, Mauna Loa, South Pole). The solid line is the geometric mean over the central two-thirds of models in each month, with the dashed lines the minimum and maximum over those central-8. The dotted line shows the minimum and maximum over all 12 models. The error bars on the observations indicate the standard deviation over the several years of data shown in Table 3.

- [Title Page](#)
- [Abstract](#) [Introduction](#)
- [Conclusions](#) [References](#)
- [Tables](#) [Figures](#)
- [◀](#) [▶](#)
- [◀](#) [▶](#)
- [Back](#) [Close](#)
- [Full Screen / Esc](#)
- [Printer-friendly Version](#)
- [Interactive Discussion](#)

AEROCOM microphysics intercomparison

G. W. Mann et al.

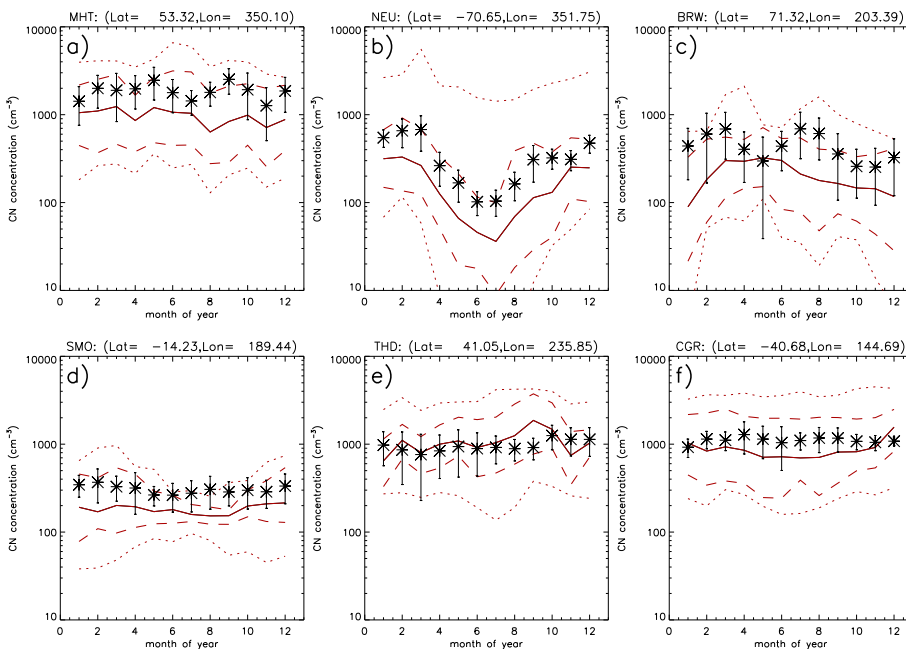


Fig. 7. Simulated annual cycle in surface $N(D_p > 10 \text{ nm}/14 \text{ nm}/3 \text{ nm})$ against CPC observations at marine boundary layer GAW sites (Mace Head, Neumayer, Barrow, Samoa, Trinidad Head, Cape Grim). The solid line is the geometric mean over the central two-thirds of models in each month, with the dashed lines the minimum and maximum over those central-8. The dotted line shows the minimum and maximum over all 12 models. The error bars on the observations indicate the standard deviation over the several years of data shown in Table 3.

AEROCOM microphysics intercomparison

G. W. Mann et al.

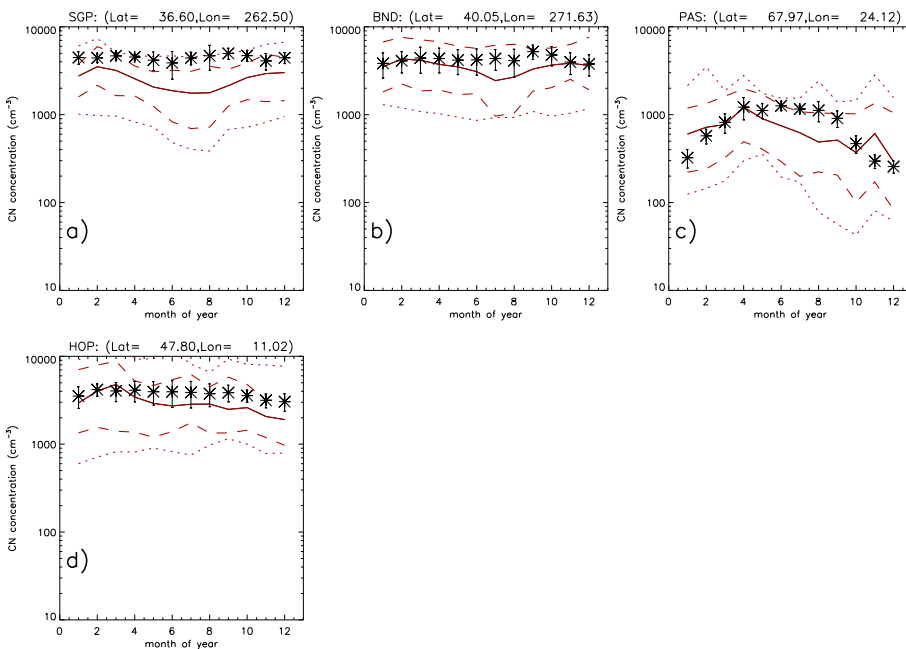
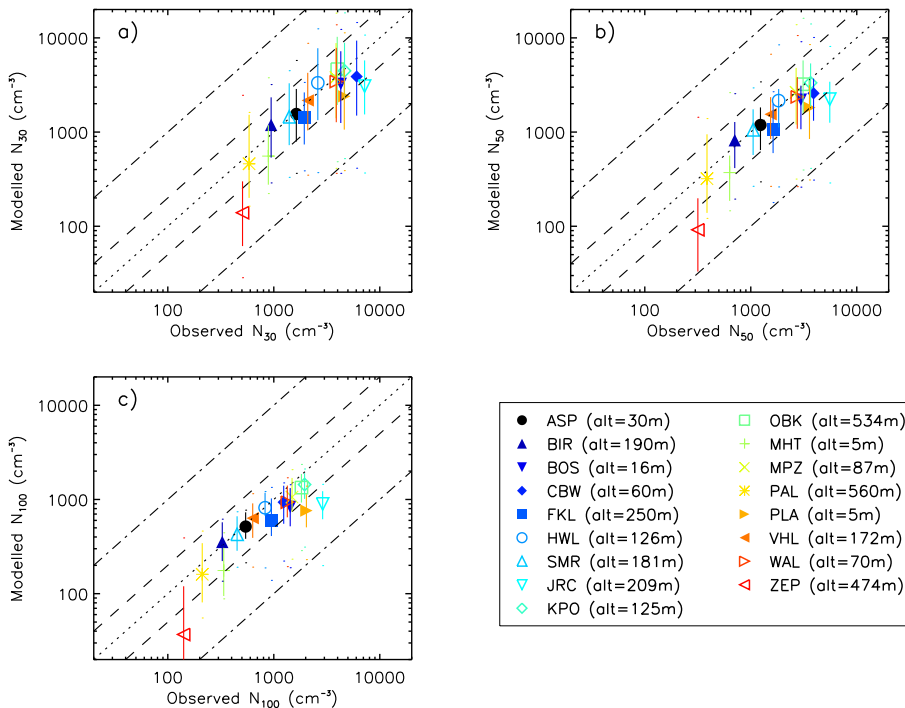


Fig. 8. Simulated annual cycle in surface $N(D_p > 10 \text{ nm}/14 \text{ nm}/3 \text{ nm})$ against CPC observations at continental boundary layer GAW sites (Southern Great Plains, Bondville, Pallas, Hohenpeissenberg). The solid line is the geometric mean over the central two-thirds models in each month, with the dashed lines the minimum and maximum over those central-8. The dotted line shows the minimum and maximum over all 12 models. The error bars on the observations indicate the standard deviation over the several years of data shown in Table 3.

AEROCOM microphysics intercomparison

G. W. Mann et al.



[Title Page](#)

[Abstract](#)

[Introduction](#)

[Conclusions](#)

[References](#)

[Tables](#)

[Figures](#)

◀

▶

[Back](#)

[Close](#)

[Full Screen / Esc](#)

[Printer-friendly Version](#)

[Interactive Discussion](#)



AEROCOM microphysics intercomparison

G. W. Mann et al.

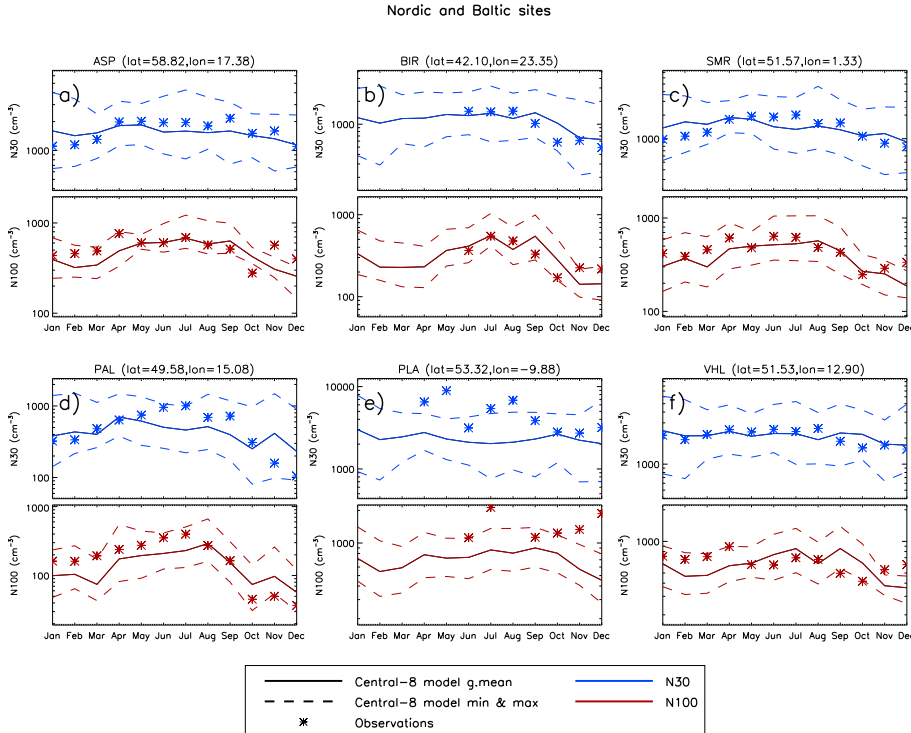


Fig. 10. Annual cycle of simulated $N(D_p > 30 \text{ nm})$ (blue), and $N(D_p > 100 \text{ nm})$ (red) against those measured by SMPS/DMPS instruments (asterisks) at the 6 Nordic and Baltic EUSAAR sites: Aspvreten (ASP, **a**), Birkenes (BIR, **b**), Hyttiala (SMR, **c**), Pallas (PAL, **d**), Preila (PLA, **e**) and Vavihill (VHL, **f**). Model values are the geometric mean (solid) and min/max (dashed) over the central-8 model monthly mean values. Observed values are arithmetic means over the hourly measurement data (A. Asmi, personal communication, 2012).



AEROCOM microphysics intercomparison

G. W. Mann et al.

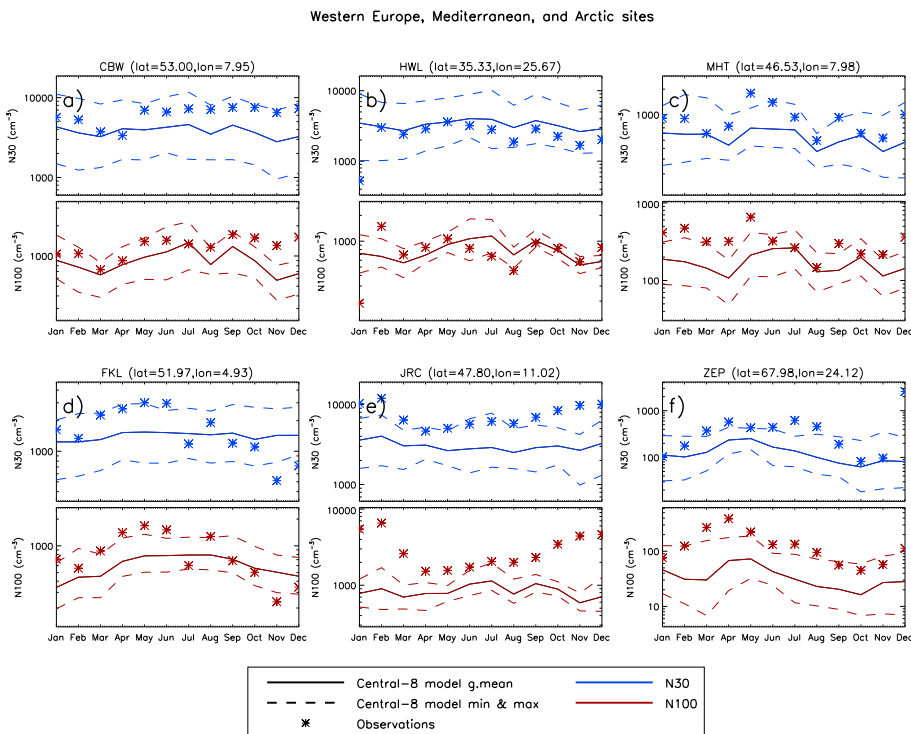


Fig. 11. Annual cycle of simulated $N(D_p > 30 \text{ nm})$ (blue) and $N(D_p > 100 \text{ nm})$ (red) against those measured by SMPS/DMPS instruments (asterisks) at the 6 EUSAAR sites classified as western Europe: Cabauw (CBW, **a**), Harwell (HWL, **b**), Mace Head (MHT, **c**), Mediterranean: Finokaklia (FKL, **d**), Ispra (JRC, **e**), or Arctic: Zeppelin (ZEP, **f**). Model values are the geometric mean (solid) and min/max (dashed) over the central-8 model monthly (arithmetic) mean values. Observed values are arithmetic means over the hourly measurement data (A. Asmi, personal communication, 2012).

AEROCOM microphysics intercomparison

G. W. Mann et al.

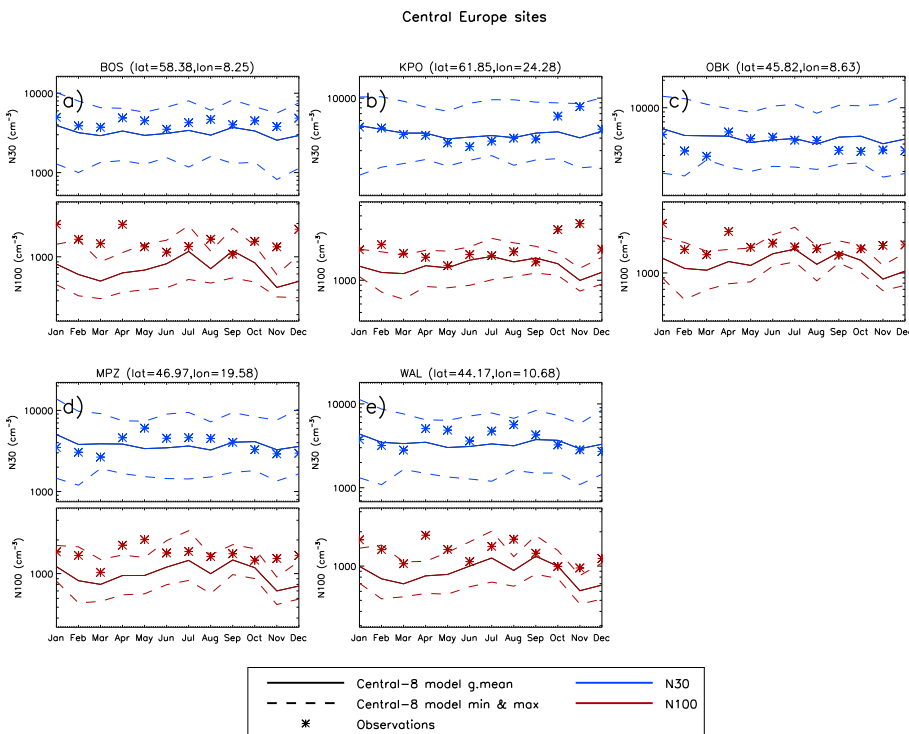


Fig. 12. Annual cycle of simulated $N(D_p > 30 \text{ nm})$ (blue) and $N(D_p > 100 \text{ nm})$ (red) against those measured by SMPS/DMPS instruments (asterisks) at the 5 low-altitude EUSAAR/GUAN sites classified as central European: Bosel (BOS, **a**), K-Puszta (KPO, **b**), Kosetice (OBK, **c**), Melpitz (MEL, **d**) and Waldhof (WAL, **e**). Model values are the geometric mean (solid) and min/max (dashed) over the central-8 model monthly (arithmetic) mean values. Observed values are arithmetic means over the hourly measurement data (A. Asmi, personal communication, 2012).

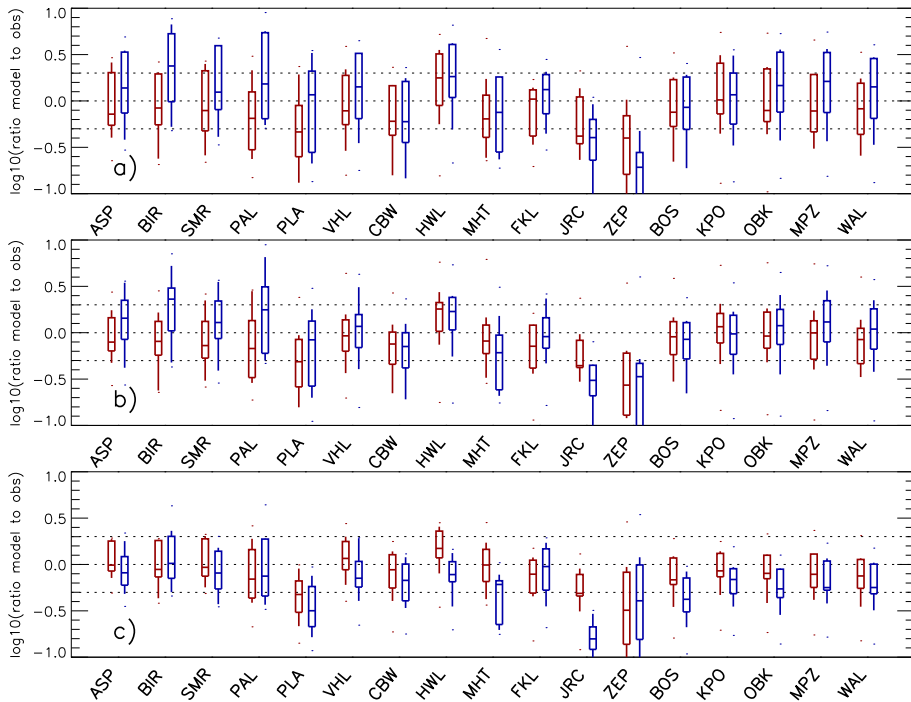


Fig. 13. Box plots indicating the median, 25th and 75th percentiles of model to observation ratio for (a) N_{30} , (b) N_{50} and (c) N_{100} at the 17 low-altitude EUSAAR/GUAN sites. Winter and summer values are shown in blue and red respectively. The plots show the base-10 logarithm of the ratio, so a value of 1.0 means a factor of 10 high bias, a value of -1.0 means a factor of 10 low bias. The dashed lines indicate where the model is within a factor of 2 of the observations.

AEROCOM microphysics intercomparison

G. W. Mann et al.

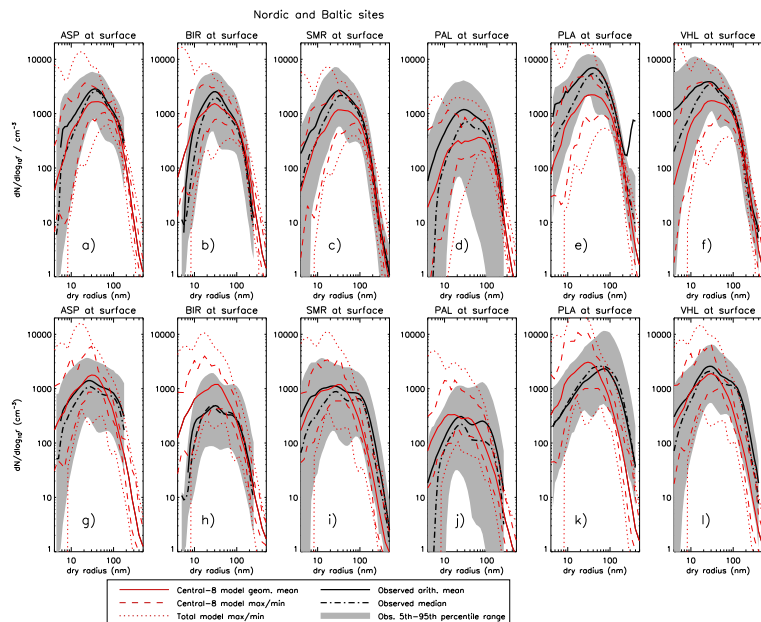


Fig. 14. Summer (**a–f**) and winter (**g–l**) multi-model simulated size distributions against DMPS/SMPS measurements at the 6 Nordic/Baltic EUAAR sites: Aspvreten (ASP), Birkenes (BIR), Hyytiala (SMR), Pallas (PAL) and Vavihill (VHL). Shown are the central-8 model geometric means (red solid), central-8 model maximum/minimum (red dashed) and all-12 model minimum/maximum (red dotted) of the June–July–August (arithmetic) mean size distributions at each site. Observed values (black solid line) are arithmetic means over the hourly measurement data (A. Asmi, personal communication, 2012). The published (Asmi et al., 2011) median (black dot-dashed) and 5th to 95th percentile range (grey shading) over the hourly measurement data are also shown for reference.

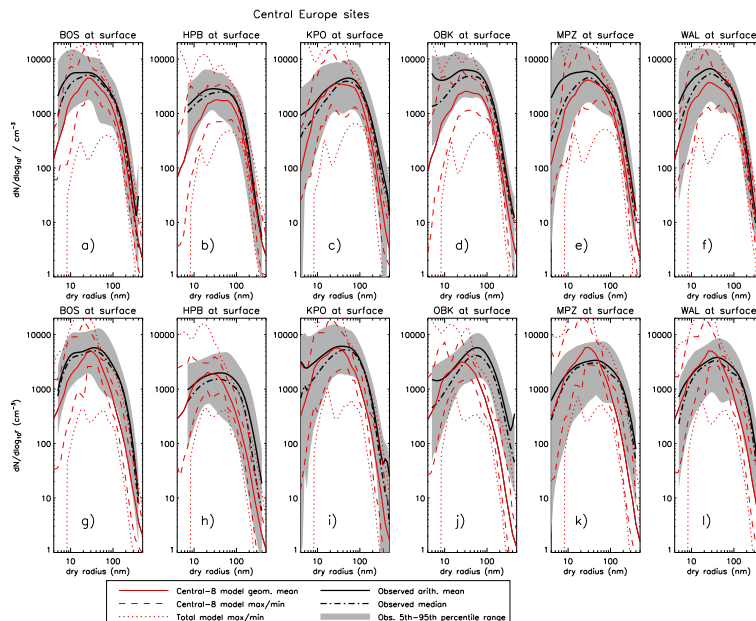


Fig. 15. Summer (**a–f**) and winter (**g–l**) multi-model simulated size distributions against DMPS/SMPS measurements at the 6 central European EUSAAR/GUAN sites: Bosel (BOS), Hohenpeissenberg (HPB), K-Puszta (KPO), Kosetice (OBK), Melpitz (MEL) and Waldhof (WAL). Shown are the central-8 model geometric means (red solid) central-8 model maximum/minimum (red dashed) and all-12 model minimum/maximum (red dotted) of the June–July–August (arithmetic) mean size distributions at each site. Observed values (black solid line) are arithmetic means over the hourly measurement data (Ari Asmi, personal communication, 2012). The published (Asmi et al., 2011) median (black dot-dashed) and 5th to 95th percentile range (grey shading) over the hourly measurement data are also shown for reference.

- [Title Page](#)
- [Abstract](#) [Introduction](#)
- [Conclusions](#) [References](#)
- [Tables](#) [Figures](#)
- [◀](#) [▶](#)
- [◀](#) [▶](#)
- [Back](#) [Close](#)
- [Full Screen / Esc](#)
- [Printer-friendly Version](#)
- [Interactive Discussion](#)

AEROCOM microphysics intercomparison

G. W. Mann et al.

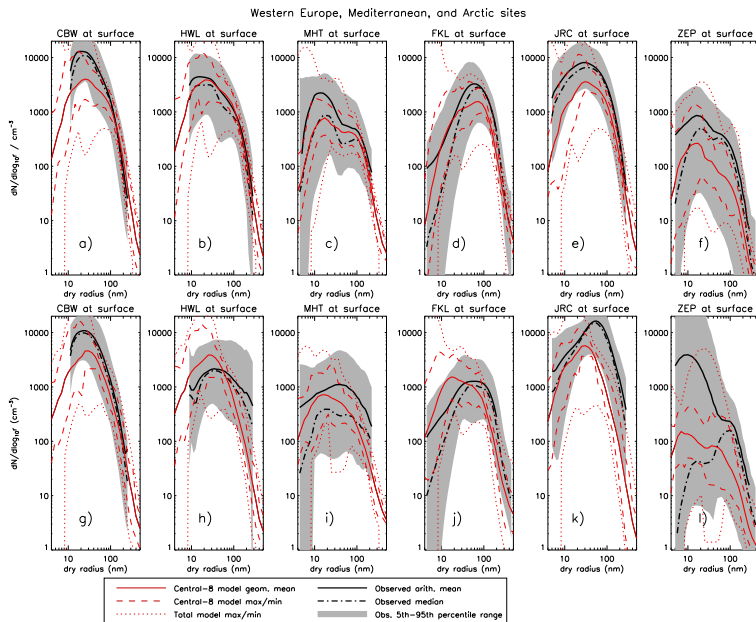


Fig. 16. Summer (**a–f**) and winter (**g–l**) multi-model simulated size distributions against DMPS/SMPS measurements at the 6 EUSAAR sites classified as western Europe: Cabauw (CBW), Harwell (HWL), Mace Head (MHT), Mediterranean: Ispra (JRC), Finokalia (FKL) or Arctic: Zeppelin (ZEP). Shown are the central-8 model geometric means (red solid), central-8 model maximum/minimum (red dashed) and all-12 model minimum/maximum (red dotted) of the June-July-August (arithmetic) mean size distributions at each site. Observed values (black solid line) are arithmetic means over the hourly measurement data (A. Asmi, personal communication, 2012). The published (Asmi et al., 2011) median (black dot-dashed) and 5th to 95th percentile range (grey shading) over the hourly measurement data are also shown for reference.

- [Title Page](#)
- [Abstract](#) [Introduction](#)
- [Conclusions](#) [References](#)
- [Tables](#) [Figures](#)
- [◀](#) [▶](#)
- [◀](#) [▶](#)
- [Back](#) [Close](#)
- [Full Screen / Esc](#)
- [Printer-friendly Version](#)
- [Interactive Discussion](#)



AEROCOM microphysics intercomparison

G. W. Mann et al.

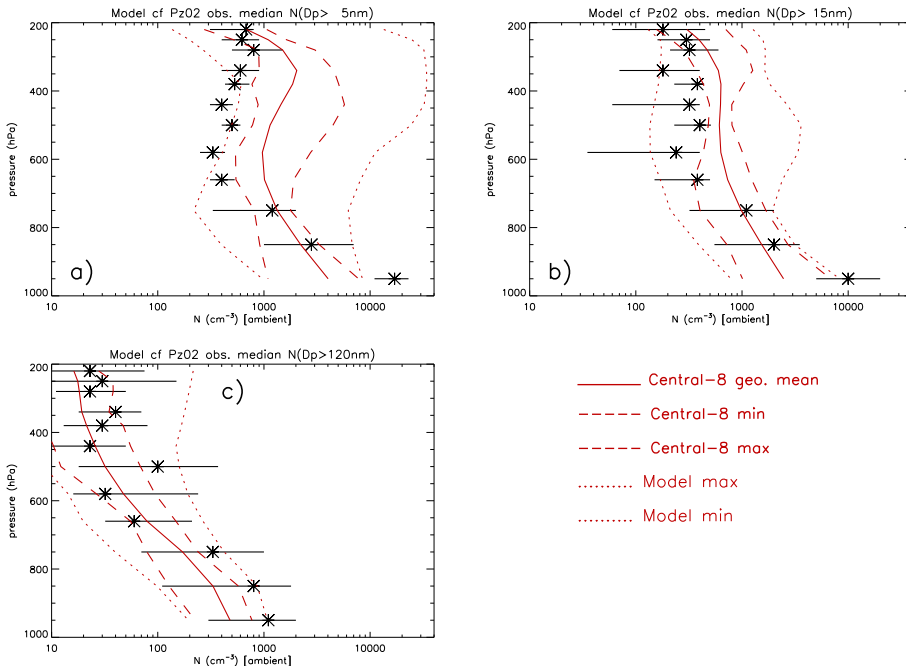


Fig. 17. Summertime central-model simulated profiles of $N(D_p > 5 \text{ nm}$, (a)), $N(D_p > 15 \text{ nm}$, (b)) and $N(D_p > 120 \text{ nm}$, (c)) over Germany against those derived from aircraft-borne CPC and PCASP measurements (asterisks) during the Lindenberg Aerosol Characterisation Experiment (Petzold et al., 2002), as presented by Lauer et al. (2005). The solid line shows the geometric mean of the central-8 models, dashed lines indicate the maximum and minimum of the central-8, while dotted lines indicate the maximum and minimum over all 12 models.

AEROCOM microphysics intercomparison

G. W. Mann et al.

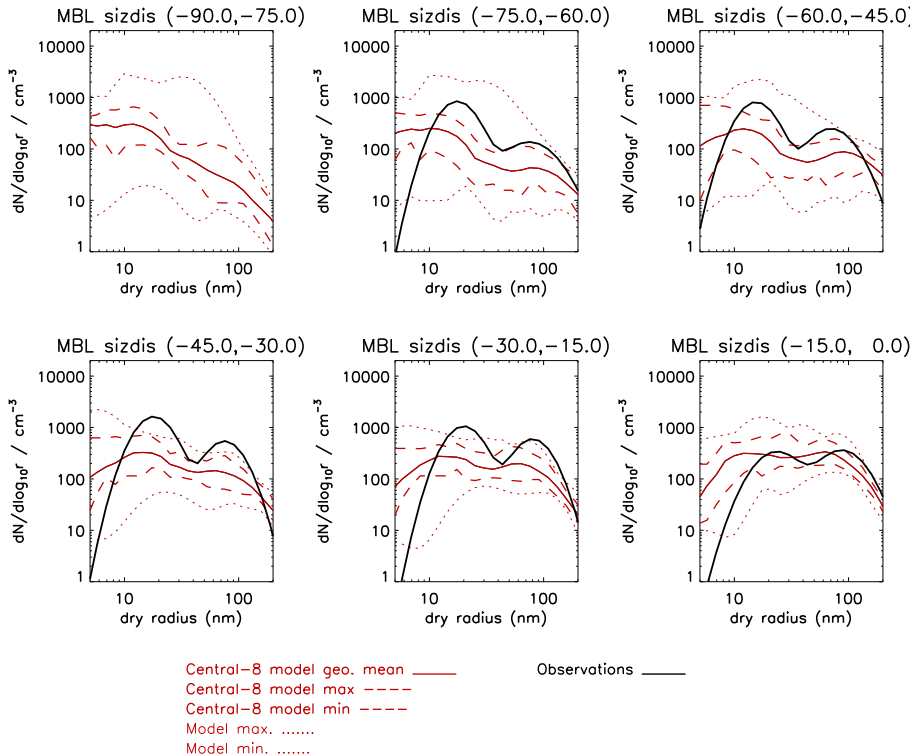


Fig. 18. Southern Hemisphere annual-mean central-model simulated size distributions in the marine boundary layer averaged into 15° latitude ranges to compare against the compilation of 30 yr of cruise DMPS/APS measurements from Heintzenberg et al. (2000). The solid line shows the geometric mean of the central-8 models, dashed lines indicate the maximum and minimum of the central-8, while dotted lines indicate the maximum and minimum over all 12 models.

AEROCOM microphysics intercomparison

G. W. Mann et al.

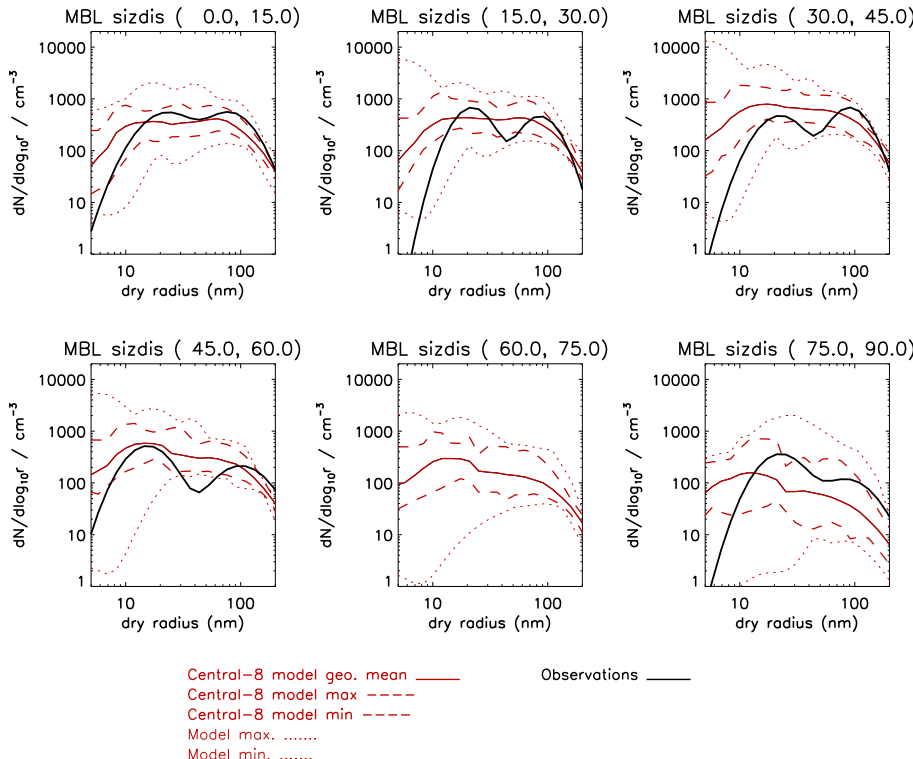


Fig. 19. Northern Hemisphere annual-mean central-model simulated size distributions in the marine boundary layer averaged into 15° latitude ranges to compare against the compilation of 30 yr of cruise DMPS/APS measurements from Heintzenberg et al. (2000). The solid line shows the geometric mean of the central-8 models, dashed lines indicate the maximum and minimum of the central-8, while dotted lines indicate the maximum and minimum over all 12 models.



AEROCOM microphysics intercomparison

G. W. Mann et al.

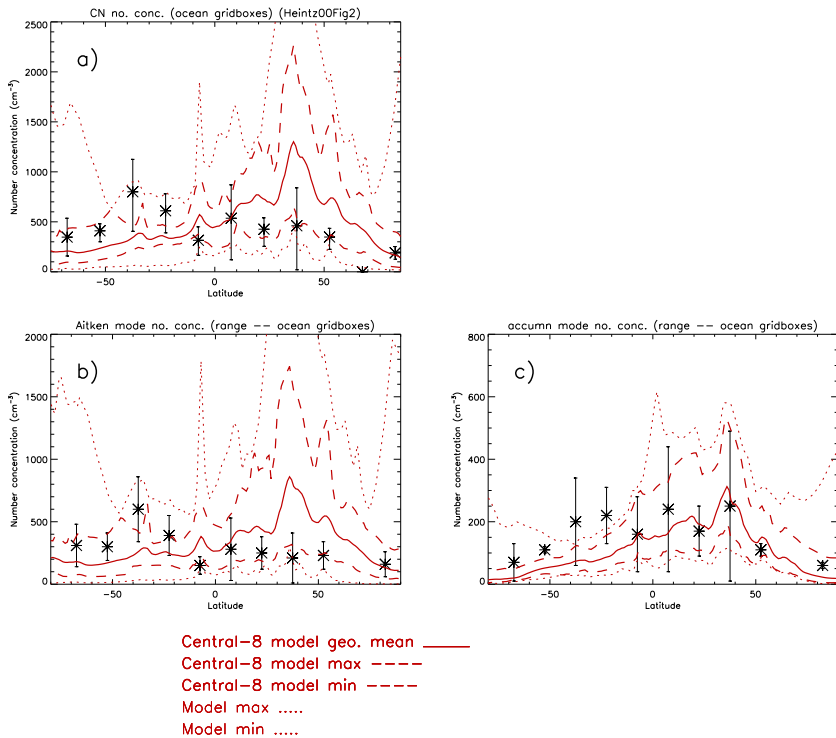


Fig. 20. Meridional variation of central-model simulated N_{10} , Aitken mode and accumulation mode particle concentrations in the marine boundary layer, compared a compilation of observations from cruise measurements (Heintzenberg et al., 2000). The observed values were derived from fitting modes to the full size distributions, whereas the model Aitken and accumulation mode concentrations are here calculated as mean $N_{10} - N_{100}$ and N_{100} respectively, averaging over all marine gridboxes in each latitude band. The solid line shows the geometric mean of the central-8 models, dashed lines indicate the maximum and minimum of the central-8, while dotted lines indicate the maximum and minimum over all 12 models.

**AEROCOM
microphysics
intercomparison**

G. W. Mann et al.

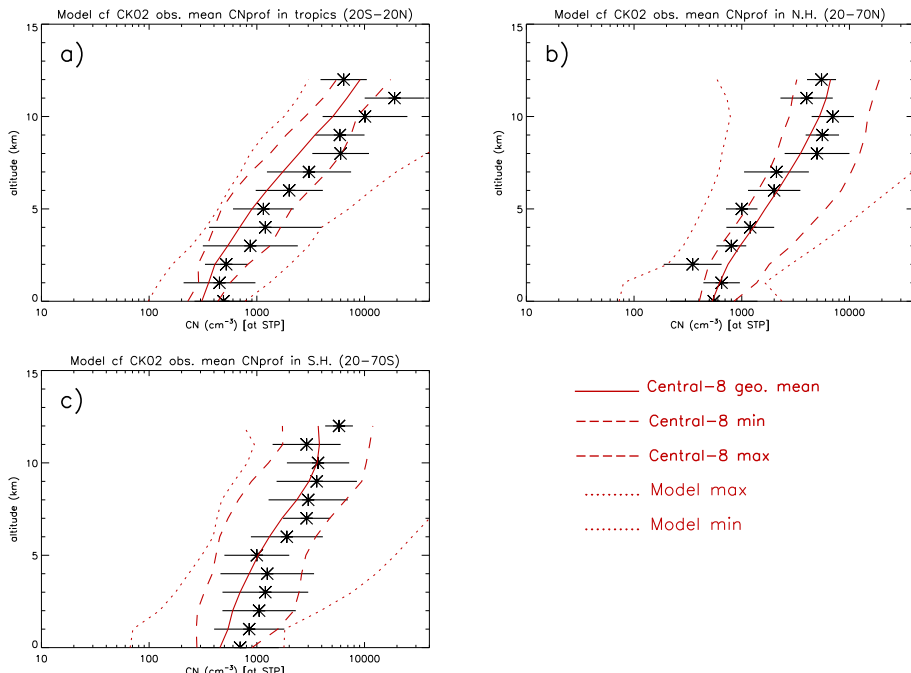


Fig. 21. Simulated vertical profile of marine size-resolved N_3 profiles over the Pacific and Southern Oceans compared to observed compilation of aircraft-borne u-CPC measurements as compiled in Clarke and Kapustin (2002). Model values are averages over gridboxes in the latitude ranges ranges 70°S to 20°S , 20°S to 20°N and 20°N to 70°N . and longitude ranges: tropical (185°W to 90°W), Northern Hemisphere (160°W to 120°W), Southern Hemisphere (135°E to 180°E). These averaged profiles for each model were interpolated onto a 1 km vertical grid. Again, since the measurements are taken over many different seasons, annual mean values were used when constructing the multi-model quantities. The solid line shows the geometric mean of the central-8 models, dashed lines indicate the maximum and minimum of the central-8, while dotted lines indicate the maximum and minimum over all 12 models.